

POLITECNICO DI TORINO

DIPARTIMENTO DI INGEGNERIA MECCANICA E AEROSPAZIALE
(DIMEAS)



SPAULDINGTM
REHABILITATION NETWORK



HARVARD
MEDICAL SCHOOL

Master's Degree Thesis in Biomedical Engineering

Advanced Machine Learning Techniques to Analyze Video Recordings for Application in Rehabilitation Medicine

Supervisors

Prof.sa Gabriella OLMO

Prof. Paolo BONATO

Candidate

Federica SEMPRONI

Torino, March 2020

Abstract

The gait function has an important impact on the quality of life of people. Nowadays numerous pathologies are the cause of a deviation from the normal gait, resulting in a great disability in the performance of the daily life activities. For this reason, the improvement of gait is one of the main focuses of rehabilitation interventions to ensure total inclusion in society and to remove every kind of barrier. Currently, motion analysis laboratories perform gait analysis using systems that exploit the tracking of infrared reflective markers positioned on anatomical landmarks of the patient. Unfortunately, these systems are cumbersome, high-cost and take a lot of hours to collect and to analyze the clinical walking data by specialized personnel.

The purpose of the thesis aims to evaluate a new marker-less approach to perform gait analysis on disabled patients by enabling low-cost, and user-friendly procedures. These techniques are based on video recordings and the use of advanced machine learning techniques to derive the position of the human landmarks used to extract the biomechanical data of the gait.

In this work, a preliminary assessment on the reliability of Openpose, a motion tracking algorithm, is performed to define the limits and to evaluate whether it will be possible the use for gait analysis. An algorithm for the extraction of the main angles of the lower limb is developed in the Matlab environment and some Openpose limits are addressed.

The comparison between Openpose, the modern tracking algorithm, and the Vicon system, the traditional motion analysis system, is carried out by studying the gait parameters of five healthy subjects.

The main objectives of this work are the comparison of the two biomechanical models, in terms of body segments-orientation and joint-angles, the comparison of the position of the centers of rotation estimated by the systems and the characterization of the Openpose estimated error in terms of angles shape, angles magnitude and markers displacement.

The final results obtained show a good estimate of the gait parameters with the use of cameras only, reporting average errors in estimating the knee and the ankle angles of less than 5 degrees, and errors in estimating the hip angle up to 10 degrees.

The preliminary evaluation of Openpose highlights the good potential for future use in the clinic of the pose estimation tool. Nevertheless, certain limits must be further exceeded to the introduction in the evaluation of patients with severe levels of disability.

Summary

This thesis work is part of a project, that is taking place at Spaulding Rehabilitation Hospital's Motion Analysis Lab, the teaching hospital for the Harvard Medical School's Physical Medicine and Rehabilitation program in Boston, that aims to validate a marker-less system for gait analysis.

The purpose of the thesis is to carry out a preliminary analysis of a pose estimation tool, called Openpose, to evaluate its possible use, in the medical field, in the context of gait analysis. The object of the present work is a comparison between the traditional system used for gait analysis, the Vicon motion capture system, and the new pose estimation tool, Openpose.

The data analyzed for the aforementioned comparison were collected by recruiting five healthy subjects, without posture and motor problems.

This document consists of six chapters, the content of which is briefly summarized below.

1. Introduction to gait analysis

This chapter provides an introduction to the work done and presented in this thesis, initially highlighting the general problem addressed, the reasons for the birth of the project itself, and subsequently presenting an introduction to gait analysis and the state of the art.

The first section shows the general problem encountered in traditional gait analyzes carried out in laboratories and introduces the innovative idea to solve the limits encountered.

The second section instead briefly reports the purpose of the general project and the specific objective of the thesis, starting from the marker-less idea.

The third section presents the basic information regarding gait analysis, considering the gait cycle and the parameters necessary for a general evaluation of the subject.

The last section reports the state of the art, which is the traditional systems used today for gait analysis, such as the simple observation of the subject by the clinicians, and the motion analysis systems such as inertial systems, video-based systems, dynamic systems, and EMG based systems.

2. Systems in comparison

In this chapter, the two systems compared in this work are presented in detail. The first system presented is considered our gold standard, as it is the most common system used for gait analysis. This is the Vicon system, a system that allows, with the use of special software, to extrapolate the parameters of the subject's gait starting from the infrared location of markers specially attached to anatomical landmarks.

The second system described is a machine learning algorithm, Openpose, which has the purpose of predicting certain landmarks on the human bodies recognized in the images provided to it.

3. Materials and Methods

This chapter describes the methods and materials used for the experiment carried out.

The first section describes the procedures and the protocol followed for the data collection, and the subjects recruited and the tools used to capture the data are presented.

The second section instead describes the steps followed for the processing of the data, with the explanation and the justification of the choice made.

4. Results and Discussion

In this chapter, all the obtained results are initially presented and then discussed.

In the first section, the results obtained from both the systems analyzed are shown, divided according to the analysis carried out: at the beginning the analysis address the positions of the centers of rotation, then the rotation of the body segments, and at last the angles of the lower limb.

In the second section, the presented results are discussed, in the same order as listed in the previous section.

5. Medical Application and Future Goals

In this chapter, in the first section, a possible medical application of the Openpose tool is introduced, considering the level of accuracy obtained.

In the second section, however, some future steps are suggested for the improvement of the Openpose output, starting from the limits and problems encountered in the preliminary analysis carried out.

6. Conclusion

In this last chapter, the final results obtained are briefly summarized, followed by some final considerations on the use of the Openpose tool.

Acknowledgements

First of all, I would like to thank Professor Gabriella Olmo for allowing me to work on this thesis under her guidance, for providing me with the precious suggestions for the success of the drafting, and for having always shown great availability.

I would also like to infinitely thank Professor Paolo Bonato for allowing me to work under his precious guide for nine months, inserting myself from the beginning in his splendid staff, making the dream of living in the USA possible and redeeming myself aware of my possible future career.

Special thanks also go to Federico Parisi and Stefano Sapienza, who have always supported me, both professionally and personally by motivating me, directing me, and above all encouraging me.

A special thanks to the usual friends, who supported me in all my choices, to the high school friends, who have been following my path for years, and to the university colleagues, who shared with me the most beautiful and difficult moments of these years of Polytechnic.

My heartfelt thanks go to my family, who made this success possible, supporting me in all my decisions and making every dream possible, without which you wouldn't know the person of today.

To my family and Jeansy

Table of Contents

List of Tables	XI
List of Figures	XIII
Acronyms	XVII
1 Introduction to gait analysis	1
1.1 General problem	1
1.2 Aim of the thesis	2
1.3 Background information	2
1.4 State of the art	7
2 Systems in comparison	10
2.1 VICON motion capture system	10
2.2 OPENPOSE pose estimation tool	18
3 Materials and Methods	25
3.1 Protocol and Procedures	25
3.2 Data analysis	27
3.2.1 Rectification of the video recordings	27
3.2.2 Definition of the scale factor to convert meter to pixel	31
3.2.3 Definition of the new reference system	33
3.2.4 Processing of OPENPOSE trajectory signals	35
3.2.5 Extraction of angles from the position of the key-points	37
3.2.6 Assessment of the length of the body segments	42
4 Results and Discussion	46
4.1 Results	46
4.1.1 Position of the centers of rotation	47
4.1.2 Orientation of the body segments	48
4.1.3 Angles of the lower limb	49

4.2	Discussion	55
4.2.1	Position of the centers of rotation	55
4.2.2	Orientation of the body segments	58
4.2.3	Angles of the lower limb	60
5	Possible Medical Application and Future Goals	61
5.1	Medical application	61
5.1.1	Cerebral palsy disease	61
5.2	Future goals	64
6	Conclusion	67
A	Guide to using Openpose	69
B	Guide to using the Camera Calibration Matlab tool	71
	Bibliography	76

List of Tables

3.1	General information on the recruited subjects	25
3.2	Walking speeds for the treadmill sessions	26
3.3	Lenses parameters of the Bonita cameras	31
3.4	Treadmill markers position for subject 1, 2, and 3	33
3.5	Treadmill markers position for subject 4, and 5	33
3.6	Treadmill length (both in meter and pixel), and scale factor values computed for the five subjects	34
3.7	Values of the window length used for the median filter, and cut-off frequencies of the low-pass filter	36
3.8	Reference values of the angles obtained by the static position for each subject	42
3.9	Values of the thigh and shank lengths for each subject considering the static position	43
4.1	Number of available steps for each subject	46
4.2	Distance, in meters, of the estimated Openpose landmarks and the Vicon centers of rotation	47
4.3	Euclidean distance, in meters, of the estimated Openpose landmarks and the Vicon centers of rotation	48
4.4	Mean value, standard deviation, maximum and minimum values of the differences in the thigh orientation for each subject	49
4.5	Mean value, standard deviation, maximum and minimum values of the differences in the shank orientation for each subject	49
4.6	Mean value, standard deviation, maximum and minimum values of the differences in the foot orientation for each subject	50
4.7	The average distances between the hip angles provided by the Vicon system and the hip angles calculated with the method used for this thesis work	50
4.8	Maximum values of the distance between the Vicon angles and the correspondent angles calculated by using the method in the paragraph 3.2.5 for each subject	54

4.9	Average RMSE values obtained from the Vicon angles and the correspondent angles calculated by using the method in the paragraph 3.2.5 for each subject	55
4.10	Average values of the distance between the Vicon angles and the Openpose angles calculated by using the method in the paragraph 3.2.5 for each subject	56
4.11	Average RMSE values obtained from the Vicon angles and the Openpose angles calculated by using the method in the paragraph 3.2.5 for each subject	56

List of Figures

1.1	Schematic division of the gait cycle [2]	4
1.2	Anatomical planes	5
1.3	Degrees of freedom of the lower limb joints	6
2.1	An example of Passive Markers	12
2.2	Positioning of VICON cameras in the Motion analysis lab at Spaulding Rehabilitation Hospital in Boston	13
2.3	Bonita Camera for VICON system	13
2.4	Active Wand for VICON system [9]	14
2.5	Creation of skeletal pelvis segments [11] (a) The first marker defines the location of one point (b) Two markers define a line (c) Three non co-linear markers define a plane (d) Four markers enable occluded markers to recreate the structure based on available markers	16
2.6	Vicon Nexus Joint centers position of the Plug-in Gait [12]	17
2.7	Visual 3D picture	18
2.8	Openpose Pipeline [13]: (a) Input Image (b) Part Confidence Map (c) Part Affinity Fields (d) Bipartite Matching (e) Parsing Results	19
2.9	Openpose multi-stage Convolutional Neural Network Architecture [13]	20
2.10	Example of Refinement of PAFs across stages [13]	21
2.11	Part association [13]	22
2.12	Graph matching [13]: (a) Part detection (b) K-graph (c) Tree structure (d) Bipartite graph	24
2.13	An example of the Openpose Output from a lateral view of the subject	24
2.14	An example of the Openpose Output from a frontal view of the subject	24
3.1	Definition of the role of extrinsic and intrinsic parameters [15]	28
3.2	Illustration of how a camera works [15]	28
3.3	Extrinsic parameters of the camera [15]	29
3.4	Pixel skew definition [15]	29
3.5	Types of radial distortion in pictures [15]	30
3.6	Types of tangential distortion in pictures	30

3.7	Pictures, both distorted and undistorted, of the Motion Analysis Lab at Spaulding Rehabilitation Hospital in Boston	32
3.8	Illustration of both the reference systems, above for the VICON system, and below for the OPENPOSE pictures. In red the new reference system used and in blue the position of the markers placed on the treadmill	34
3.9	Raw trajectories, step by step, of the y-coordinate of the leg joints: hip, knee, and ankle (subject 1)	35
3.10	Raw trajectories, step by step, of the y-coordinate of the foot joints: heel, median toe, and lateral toe (subject 1)	35
3.11	Masks of the three different filters (a) Butterworth (b) Chebyshev (c) Elliptic	37
3.12	Effect of the median filter on the original signal. It shows the trajectory of the hip, knee, and ankle coordinate of subject 1 during fast walk (subject 1)	38
3.13	Residual analysis of a trajectory signal to find the correct cutoff frequency (subject 1)	38
3.14	Result of the Chebyshev filter applied on the trajectory signal (subject 1)	39
3.15	Filtered trajectories, step by step, of the y-coordinate of the leg joints: hip, knee, and ankle (subject 1)	40
3.16	Filtered trajectories, step by step, of the y-coordinate of the foot joints: heel, median toe, and lateral toe (subject 1)	40
3.17	Bio mechanical definition of the hip, knee, and ankle angles	41
3.18	Definition of the hip angle	41
3.19	Median confidence of the Openpose system for one subject (subject 1)	44
3.20	Representation of the method to reconstruct the leg by considering constant segment lengths	45
4.1	Hip, knee, and ankle angles provided by the Vicon system (subject 1)	51
4.2	Hip, knee, and ankle angles obtained from the positions of the centers of rotation provided by the Vicon system (subject 1)	51
4.3	Median distance and standard deviation between the angles provided by the Vicon system and the angles obtained with the method described in paragraph 3.2.5 (subject 1)	52
4.4	Hip, knee, and ankle angles provided by the Vicon system, in blue, and angles obtained with the method described in this thesis, in red.	52
4.5	Hip, knee, and ankle angles provided by the Vicon system, in blue, and corrected angles obtained with the method described in this thesis, in red.	53

4.6	Median distance and standard deviation between the angles provided by the Vicon system and the angles obtained with the method described in paragraph 3.2.5, after compensating the bias in the hip angles	53
4.7	RMSE calculated for each step, between the Vicon angles and the correspondent angles calculated by using the method in the paragraph 3.2.5 (subject 1)	54
4.8	Hip, knee, and ankle angles obtained starting from the positions of the predicted landmarks provided by the Openpose tool (subject 1)	55
4.9	Hip, knee and ankle angles provided by the Vicon system, in blue, and Openpose angles obtained with the method described in paragraph 3.2.5, in red (subject 1)	57
4.10	Median distance and standard deviation between the angles provided by the Vicon system and the Openpose angles obtained with the method described in paragraph 3.2.5 (subject 1)	57
4.11	Hip, knee and ankle angles provided by the Vicon system, in blue, and Openpose angles obtained with the method described in paragraph 3.2.5, in red (subject 2)	58
4.12	Median distance and standard deviation between the angles provided by the Vicon system and the Openpose angles obtained with the method described in paragraph 3.2.5 (subject 2)	58
4.13	Hip, knee and ankle angles provided by the Vicon system, in blue, and Openpose angles obtained with the method described in paragraph 3.2.5, in red (subject 5)	59
4.14	Median distance and standard deviation between the angles provided by the Vicon system and the Openpose angles obtained with the method described in paragraph 3.2.5 (subject 5)	59
5.1	Example of a session of a child with CP in the Motion Analysis Lab at the Spaulding Rehabilitation Hospital	62
5.2	Example of the Openpose output of a child with CP in the Motion Analysis Lab at the Spaulding Rehabilitation Hospital	63
5.3	Example of the Openpose output of a child with CP in the Motion Analysis Lab at the Spaulding Rehabilitation Hospital	63
5.4	Guidelines table for classifying CP patients according to the Edinburgh scale [17], considering the lower limb angles during the stance phase of the GC	65
5.5	Guidelines table for classifying CP patients according to the Edinburgh scale [17], considering the lower limb angles during the swing phase of the GC	65

5.6	Example of the 3D reconstruction, by the Openpose tool, of the body skeleton starting from different cameras and different points of view [18]	66
A.1	BODY-25 model [13]	70
A.2	COCO model [13]	70
B.1	The first screen of the application: the images, in which the chessboard is visible, are uploaded	72
B.2	The second screen of the application: window for the definition of the size of the chessboard squares	72
B.3	The third screen of the application: window showing the chessboard detection result	73
B.4	Result of the chessboard detection	73
B.5	Calibration of the instrument	73
B.6	Results in term of reprojection errors	74
B.7	Results in term of camera and pattern centric	74
B.8	Image without distortions	74
B.9	Export of calculated final parameters	75
B.10	An example of chessboard that can be used for the calibration of the Bonita cameras	75

Acronyms

EMG

Electromyography

GC

Gait cycle

PAF

Part Affinity Field

2D

Two dimensions

3D

Three dimensions

CNN

Convolutional neural network

LED

Light-emitting diode

DOF

Degrees of freedom

IK

Inverse kinematics

RHS

Right heel strike

RTO

Right toe off

RMSE

Root mean square error

CP

Cerebral palsy

Chapter 1

Introduction to gait analysis

1.1 General problem

The gait function has an important impact on the quality of life of children and adults. Several pathologies, such as spinal cord injury, brain injury, stroke, amputation, neuromuscular disorders, cerebral palsy, etc. are some of the numerous causes of the deviation from the normal gait. Due to the spread of the previous disorders, the improvement of gait is one of the main focuses of rehabilitation interventions. The goal of the rehabilitation clinics is to improve the disabled patients' quality of life, to ensure total inclusion in society, to obtain equal opportunities in everyday life and remove every kind of barriers.

Nowadays the main clinic purpose is to perform longitudinal evaluations of the gait quality in patients undergoing rehabilitation interventions to generate surgical recommendations, to perform pre- and post- intervention assessments, to get a feedback on ongoing patient's rehabilitation and to eventually define a new plan to adjust the rehabilitation strategies if needed. Currently, motion analysis laboratories perform gait analysis using traditional camera-based systems that exploit the tracking of infrared reflective markers positioned on anatomical landmarks. Unfortunately, these systems are cumbersome, high-cost and take 2+ hours to collect clinical walking data per subject. Furthermore, additional hours are necessary for data analysis by specialized personnel. Moreover, the complexity of positioning markers on patients with such disorders should not be underestimated. All this makes the traditional systems limited access to this type of data in the clinic and makes it difficult the envision such a system to collect data longitudinally during gait intervention. For this reason, new tracking technologies are emerging to replace the traditional capture system. Simplifying the method by which performing gait analysis would bring both scientific and medical benefits, as they would allow the patient's progress to be constantly and quickly monitored.

1.2 Aim of the thesis

This thesis work is part of a larger project that is taking place at Spaulding Rehabilitation Hospital’s Motion Analysis Lab, the teaching hospital for the Harvard Medical School’s Physical Medicine and Rehabilitation program in Boston.

The purpose of the project aims to develop a new marker-less approach to perform gait analysis on disabled patients by enabling low-cost, user-friendly procedures that could take a fraction of the time currently necessary to the analysis of this type of data. Ideally, the idea is to provide the clinicians with the gait data throughout the intervention to allow them access to the responsiveness of each patient to the therapy and to facilitate adjustments in the intervention strategy if needed, to guarantee better care of each patient in the rehabilitative clinic. This new approach could allow making quantitative data that are useful for the clinical decision-making process, enabling a reduction in the cost of the rehabilitative assessment.

The main innovation is the use of motion tracking technologies, recently introduced in the field of computer science, that have the desirable characteristics being simple to use for motion tracking. These techniques are based on collecting data starting from standard video-cameras and, by using advanced machine learning techniques, it is possible to derive biomechanical data from the video recordings. Because of the insufficient accuracy of the previous technologies, that are not designed for clinical use, it is not possible at this time an accurate analysis of gait abnormalities. For this reason, the purpose of this thesis is to perform a preliminary assessment on the reliability of a motion tracking algorithm, the pose estimation “Openpose” tool, to define its limits and to evaluate whether it will be possible to use it for gait analysis. The final goal is to generate accurate estimates of the biomechanics of motion by adjusting the limits of the previous technology and to define if the new technology has the potential to replace the traditional motion analysis systems. In other words, this work propose an accuracy comparison between the modern tracking algorithm and a traditional system.

1.3 Background information

The gait is defined as the way a person walks.

The ability of walking plays an important role in everyday life and an incorrect posture and gait can compromise the quality of life.

In fact, due to neuromuscular, musculoskeletal conditions and painful lower limb segments, some changes can be made in one’s posture and gait that can compromise their efficiency. Normally one tends to compensate the limits in the movement of the lower limb by increasing the movements of the joints that are below and above. For this reason, it is important to first know the physiological and biomechanical

bases of a normal gait, in order to be able to analyze and define any abnormalities in a person's walk.

Walking is the method used to move that involves the use of two legs, alternately, which must simultaneously guarantee propulsion and support.

The walk consists of a sequence of repetitive movements that allow us to advance and maintain the balance of the body. For this reason, good coordination and functionality are required in the segments of the lower limbs during all phases of the gait. During the advancement, two roles of the lower limbs alternate: one leg moves forward to reach a new foothold while the other leg acts as a source of support.

A single sequence of these actions by one leg is called the Gait Cycle [1].

As shown in figure 1.1, the gait cycle is composed of two phases and it is defined as the period time between two successive occurrences of the same phase of the gait. The duration of an entire GC is called cycle time.

The two phases are:

1. The Stance Phase: it is defined as the period time during which the foot, which plays a supporting role in this case, is in contact with the ground. This phase begins with the initial contact of the foot, the Heel Strike event, and lasts approximately 60% of the GC.
2. The Swing Phase: it is defined as the period time during which the foot is in the air and the leg advances. It begins when the foot comes off the ground, the Toe Off event, and it lasts about 40% of the GC.

To allow the body to perform the main functions for walking, there must be some alignment in the stance phase between the body and the foot, which performs the support function, simultaneously with the advancement of the other limb. This is made possible by a series of functions performed by the hip, knee and ankle joints. Since the angles formed by the lower limb segments are very significant for the success of the walk, they can be an indicator for interpreting the effects of disabilities on a person's gait. The result of the reaction of the aforementioned joints allows the lower limb to perform three important walking tasks [3].

The classic event-based step division may be inappropriate for some patients with varying degrees of disability.

For this reason, at the Rancho Los Amigos Medical Center, the new step division system has been defined, also applicable to pathologies that can invalidate, based on the purpose of these three tasks of the step [4]:

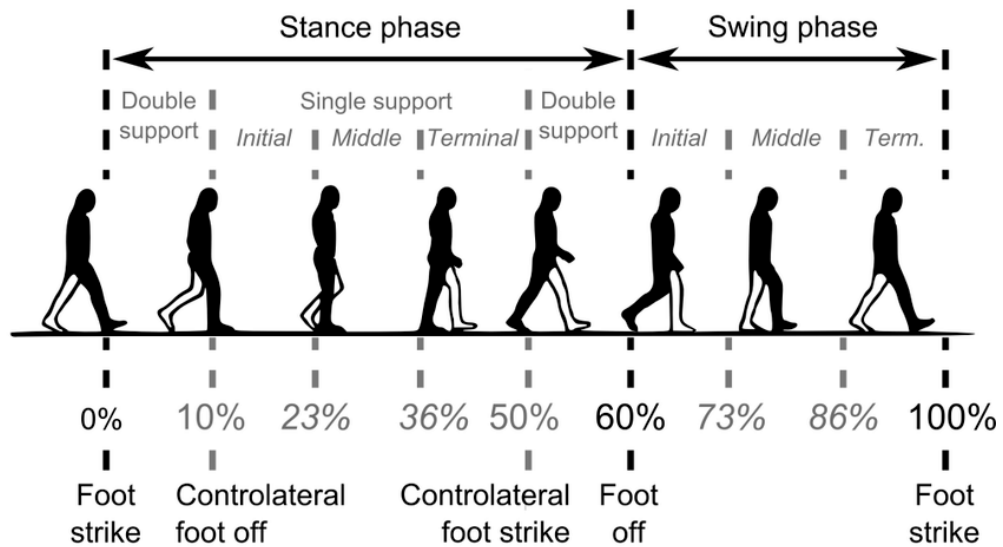


Figure 1.1: Schematic division of the gait cycle [2]

1. Weight Acceptance: the transfer of the bodyweight happens onto the limb that has just finished the phase of the swing;
 - Initial Contact(0-2%): the foot just touches the floor to begin the stance phase; the hip is flexed, the knee is extended, and the ankle is dorsi-flexed to neutral;
 - Loading Response(2-12%): the bodyweight is onto the forward limb to begin the double stance phase; the hip is flexed for stability, the knee is flexed for shock absorption, and the ankle is plantar-flexed;
2. Single Limb Support: a single limb has the responsibility of the bodyweight;
 - Mid-Stance(12-31%): the limb advances over the stationary foot; the ankle is dorsi-flexed, the hip and the knee are extended;
 - Terminal Stance(31-50%): the bodyweight moves ahead of the forefoot; the hip increases the extension, the knee increases the extension and then begins to flex lightly, and the ankle is dorsi-flexed;
3. Limb Advancement: the limb advances during the swing phase;
 - Pre-Swing(50-62%): final phase of stance; loss of hip extension, powered plantar-flexion and increased knee flexion;
 - Initial Swing(62-75%): first one-third of the swing phase; foot lifted partially dorsi-flexed, hip flexion helps the progression of the limb, increasing of knee flexion;

- Mid-Swing(75-87%): advancement of the limb in air; the hip is flexed, the knee is extended in response to the gravity and the ankle is dorsi-flexed to neutral;
- Terminal-Swing(87-100%): final phase of the swing; the hip is flexed, the knee is extended and the ankle is dorsi-flexed.

For a complete analysis of the gait, the subject under examination must be observed by the clinicians during walking from different points of view, which are the front, behind and side [5]. These perspectives allow investigating the different movements of the joints on the three anatomical planes. The planes are defined starting from the anatomical position of the body (erect head, gaze and palms of the hands facing forward, arms at the sides, fingers of the hands stretched out, feet facing forward and perpendicular to the body): the sagittal plane runs in anterior-posterior position dividing the body into two symmetrical parts, right and left; the frontal (or coronal) plane, perpendicular to the sagittal plane, runs in a lateral-lateral position dividing the body in anterior and posterior part; the transverse (or axial) plane divides the body into an upper and lower part (figure 1.2).

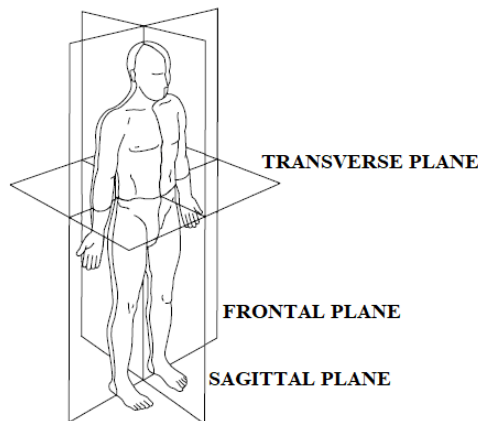


Figure 1.2: Anatomical planes

For the gait analysis, the lower limb's segments and joints are mainly observed. The lower limb is composed of three segments: the thigh that is the proximal segment, the shank that is the intermediate segment, and the foot that is the most distal segment. The main joints for gait analysis are three.

1. The hip welds the lower limb to the trunk via the coxo-femoral joint. It is an enarthrosis joint, characterized by a hemispherical shape of the articular

surfaces (one concave and the other one convex) and by the possibility of movements in all directions. The articular heads are the acetabulum of the hip bone, a pit filled with an adipose pad, and the head of the femur covered with cartilage. It is an articulation with three degrees of freedom: flexion-extension on the sagittal plane, adduction and abduction on the coronal plane, and internal and external rotation on the transverse plane;

2. The knee joint is the largest joint in the human body and connects the femur to the tibia, with the patella that stabilizes the joint itself. In this case, it is a trochlea articulation, or angular ginglymus articulation, in which an articular surface is in the shape of a pulley (approximately in the shape of a cylinder dug transversely in the center by a throat), whose axis is perpendicular to the diaphysis of the bone. The articular heads are the condyles and the patellar face of the femur, the articular face of the tibia and the articular face of the patella. This articulation allows two degrees of freedom: flexion-extension on the sagittal plane and internal and external rotation on the transverse plane;
3. The ankle joint also called the tibio-tarsal, is another angular ginglymus articulation. The articular heads are the lower articular face of the tibia and the articular face of the medial and lateral malleoli. It is a joint with three degrees of freedom: flexion-extension on the sagittal plane, called plantar and dorsal, adduction and abduction on the coronal plane and internal and external rotation on the transverse plane.

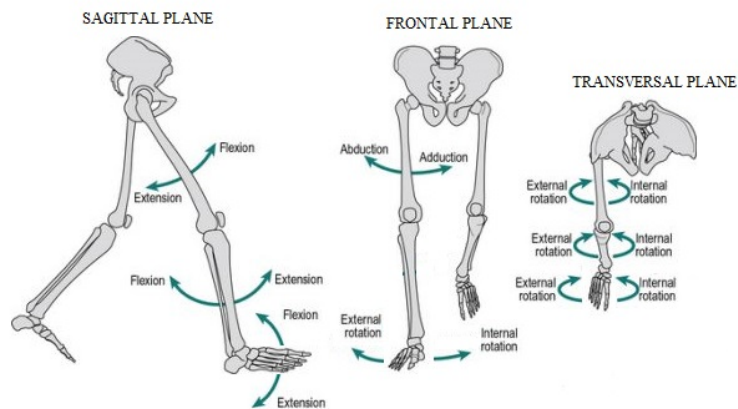


Figure 1.3: Degrees of freedom of the lower limb joints

1.4 State of the art

The study of postural control and gait have led to a significant advancement in the treatment of various pathologies and the rehabilitation of disabled people. Today there are different techniques for analyzing gait, but each form of observation of the gait individually involves some limitations in the accuracy of the assessment. Therefore, a combination of a good clinical evaluation, based on the simple observation of the walk by the clinicians, with a gait analysis, using the systems available today, can be an excellent tool for a qualitative and quantitative evaluation of the abnormalities of the gait. The advancement of bio-engineering technology in this area allows continuous improvements in the analysis of the characteristics of the gait. Different types of analysis can be considered: the kinematic analysis allows to obtain information regarding the pure motion of the body points, thus obtaining the joint angles, the angular speeds and the angular accelerations of the main lower limb joints; the kinetic analysis allows to obtain information on the causes of the movement of a body, therefore to obtain information on the joint forces, moments, and powers; besides, the dynamic analysis of electromyographic activity and the analysis of energy consumption add important information on the gait of a subject.

1. Observational gait analysis: the simple observation, without the use of tools and equipment, of walking is an excellent tool used by clinicians for a first assessment of the subject. An effective observation is carried out by systematically focusing on a single part of the body at a time. The first limitation of this technique is the inability to simultaneously observe the relationship between different body segments and to be able to identify abnormalities of the step by eye in a short period time. Besides, for a good assessment of the gait, the simultaneous assessment of the subject from different points of view would be necessary.
2. Gait analysis systems: for a better assessment of gait and postural control, there are several tools and equipment that provide this type of clinical data [6][7].
 - Inertial Motion Tracking Systems. There are several types of sensors that can be used for direct recording of kinematic variables while walking. In particular, gyroscopes are used in inertial systems (they provide the measurement of angular speeds or the rotation angles of a moving body), accelerometers (they provide an electrical signal proportional to the applied acceleration), inclinometers, etc. For gait analysis, portable systems are often used which contain these sensors inside. The device is positioned directly on the body segment to be investigated and normally has a good

form factor, which makes them usable even for disabled patients. The choice is normally limited to miniaturized devices, so as not to disturb movement and so that they can also be applied to small parts of the body, not expensive and with good performance. Having to be applied directly to the body, they suffer from the limitations described above for the markers: the criticality in positioning on certain subjects, the choice of the positioning area and the poor mechanical stability of the devices can adversely affect the measurements taken.

- Video-based automated Motion Tracking Systems. These systems are among the most accurate systems for gait analysis on the market today. These are systems consisting of markers (in the shape of small hemispheres or small spheres), active or passive, which are positioned on the subject's landmarks and cameras placed in the laboratory. They are characterized by a good resolution, defined based on the ability to distinguish the position of the markers in terms of space and time. In the case of passive reflective markers, covered with reflective adhesive material, a direct light source is not necessary to power them, but they require the presence of an infrared lighting source (to not disturb the patient) at regular intervals, placed close or above each camera, to be identified during the session by the coaxial camera. Among the most common passive marker systems are Ariel, Vicon, Elite, etc. In the case of actively illuminated markers, we can describe them as small bulbs, we consider optoelectric markers that require a direct source of illumination, normally LED. Among the most popular systems that use these markers are Selspot, Watsmart, and Optotrak. In both cases, more than one video camera is used, at least two, for 3D tracking of the points of the body in movement by the use of stereophotogrammetry procedures. They require an initial system calibration and an algorithm for the identification of the coordinates of the marker position and the centers of rotation of the joints. In addition, a guide is required for the positioning of the markers on the body, depending on the system and the biomechanical/mathematical model that is intended to be used for the study of the gait. There are some problems related to the use of these systems: first of all, on a practical level, they are cumbersome, expensive and take a long time for the data collection. Furthermore, an "ad hoc" environment is required for its use, which makes it not usable directly in the clinic. In addition, there are some sources of uncontrolled errors such as the critical positioning of the markers with respect to the subject's anatomy (especially if it is children or subjects with strong physical disabilities), the movement of the markers on the skin during movement and the possibility that for a few moments not

all the markers are visible from the system. If a marker is not visible by at least two cameras simultaneously, its position is estimated by an algorithm. The main causes of this visual obstruction are the passage of the upper arm in front of the hip during the swing phase and the use of assistive-devices during walking [8].

- Video-based markerless Motion Tracking Systems. It is a modern category of systems that are becoming useful in research. They are systems in which markers or other types of equipment are not used, but simply standard video-cameras. With the use of software, recently introduced in the field of computer science, the movement of the recorded body is reconstructed. These are inexpensive, not cumbersome systems that can be applied to any category of subject, including patients with severe disabilities. Nowadays the limitation of these pose estimation tools is poor accuracy in the recognition of body points. Also in these systems, several cameras can be used to simultaneously investigate the sagittal and coronal plane of motion. By merging the data from at least two cameras it can be possible the 3D reconstruction of the coordinates of the body joints.
- Dynamic Motion evaluation Systems. The dynamometric methods exploit the use of platforms and force platforms on which the subject is made to walk. They consist of sensor arrays placed on the surface of the laboratory, or directly in the subject's shoes, to record the pressure and force exerted by the body during walking. The three components of the forces recorded as the final result or individually are studied. These techniques are often used for clinical or sports evaluations.
- Electromyographic Motion evaluation Systems. Electromyographic techniques measure the electrical activity of the muscles during walking. EMG signals are exploited by the overlap of multiple motor units that are recruited to perform a certain movement. To take the EMG trace, surface sensors are used, positioned directly on the skin in correspondance of the muscle to be investigated and take the overall muscle activity, or invasive electrodes for greater selection of the motor units to be recorded. With the use of multichannel systems, today it is possible to reduce the artifacts acquired during registration.

Chapter 2

Systems in comparison

The main idea, on which this thesis project is based, is to assess whether the attractive motion tracking technologies, recently introduced in the field of computer science, have adequate accuracy to be able to extrapolate information on the posture and gait of subjects suffering from different degrees of disability due to numerous pathologies.

In this chapter the two systems to be compared are therefore introduced: the VICON motion capture system, that is the traditional system used today in gait analysis laboratories and considered the gold standard for this thesis work, and OPENPOSE, a recent tool of pose estimation that is taking hold in various areas for the recognition of human bodies in video recordings.

2.1 VICON motion capture system

The VICON system is a motion tracking tool widely used in research laboratories, as it is among the most accurate systems on the market for this purpose.

Despite the high cost of the equipment, the time required for both the data collection and the data analysis, and the difficulty in preparing the subject to be analyzed, it is still the most used system for both posture and gait analysis, for rehabilitation purposes and research in different fields, such as sports, medicine, etc. Nowadays it is the designed and clinically validated system for posture balance and gait analysis. As previously reported, the system requires a laboratory specifically designed for its use.

In this paragraph the equipment necessary to prepare an environment for the VICON system is described, the various equipment on the subject for data acquisition are presented and the necessary software for the analysis of the collected data are introduced. The system is widely used in rehabilitative clinics and its importance is due to the several main purposes of its use: to perform evaluations of the gait

in subject undergoing interventions, to define surgical recommendations and to generate pre- and post- intervention assessments.

In particular, the VICON system analyzes the position of the markers in the subject's landmarks to reconstruct the walk, to provide clinicians with the necessary data for its analysis and to measure the forces of the ground while the subject performs motor tasks.

Necessary equipment for data acquisition

This paragraph lists the necessary equipment for the acquisition of the motor task data, during the performing session, by the optometric system.

1. **Markers.** The markers are small objects in the spherical shape that must be positioned on the subject body in several defined key points. Depending on the VICON cameras type, two kinds of markers can be used to recognize the landmarks of the subject, during the gait or posture session, that are the active or the passive markers. The active markers are visible light-emitting diodes whose light is captured by the cameras to track the position of the markers. To increase the contrast ratio in the image a partial dark environment is required. Each marker can be composed of an array of different LEDs that are captured by the cameras, in the best case, as a single light circle. The captured light may not appear as spherical on certain camera views. In addition, a power supplier is necessary to be sure to capture them during the whole session [8]. Since each marker can have a different colored light or can be turned on or off at different instants, the data tracking phase is simplified; however, these systems have not had the commercial success of passive marker systems. On the other hand, the passive retro reflective markers, shown in figure 2.1, are small objects covered by reflective adhesive film. To trace the position of this type of marker, infrared light-emitting cameras are required. The retro-reflective markers reflect the infrared flashing light coming from the cameras and, in this way, the position is traced during the body movements. In this thesis work, passive markers were used to collect the data. Different types of markers positioning on the body are provided, depending on the purpose of the study and the data to be extrapolated from the acquisition. If possible, it is advisable to place the markers not too close to each other, as merged reflections to the cameras can return inaccurate centroid location, or they can be discarded by the circularity filter.
2. **Force plates.** In the gait analysis laboratory the synchronized force platforms, in the walkway position, are useful to enable the kinetic data captured during the acquisition of gait data generated by the moving or standing subject. The plates detect the ground-reaction forces to have information about posture,



Figure 2.1: An example of Passive Markers

balance, gait, strength asymmetries, compensatory strategies, etc. of a subject. It is possible to define the center of gravity, that is the location in which the vertical ground reaction force is located and it is equal and opposite to the downward-acting forces. The system can transduce in force or moment, it depends on the platform, the output of different kinds of sensors, such as strain gauge, capacitance gauge, piezoelectric sensors, piezoresistive sensors, etc. In figure 2.2, the position of two force platforms (at Spaulding Rehabilitation Hospital's Motion analysis Lab), squares with numbers one and two, is shown.

- 3. VICON Motion Capture Cameras.** Since passive markers are used for this thesis work, the cameras that record the subject in the motion capture volume must be infrared. The cameras are positioned around the space to be framed. At least two cameras are necessary to reconstruct the 3D coordinates of the markers, but generally, a dozen cameras are placed in the VICON space to be sure that, in any moment, at least two cameras can capture the reflective light of each marker, to avoid the occlusion. Before the gait session, the infrared cameras should be calibrated. Figure 2.2 shows an example of the position of the infrared cameras, marked with blue dots, in a motion analysis laboratory (in particular, at Spaulding Rehabilitation Hospital's Motion analysis Lab). For a good marker tracking, it is suggested to adjust the focus and to position the cameras not too far from the target object. To obtain good results, in terms of spatial coordinates of the position of the markers, these must be observed by the cameras from a great variety of different and unique positions. To ensure good accuracy in the results, the cameras must be perfectly stationary, therefore positioned on a motionless fixed support. Any slight deformation or fluctuation of the support influences the precision of the cameras detection.
- 4. Standard cameras.** Some additional standard cameras are placed in the motion analysis laboratory to record the session, as figure 2.2 shows (these cameras are marked with red dots). These cameras can be useful to validate

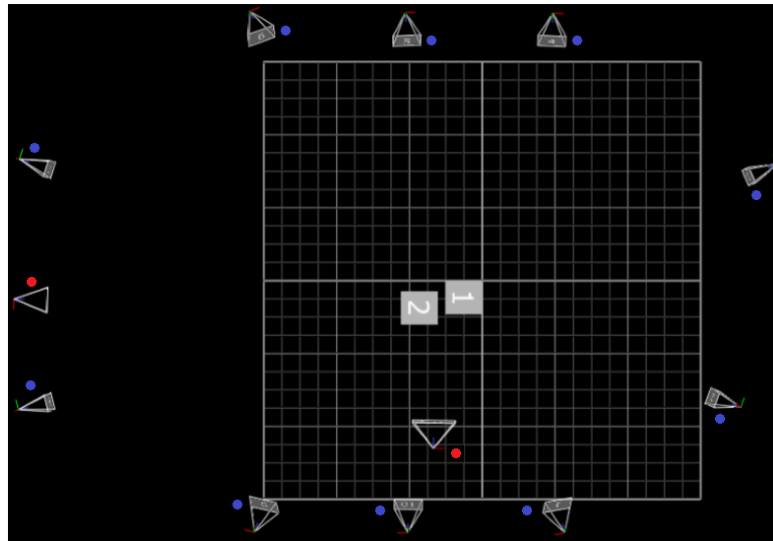


Figure 2.2: Positioning of VICON cameras in the Motion analysis lab at Spaulding Rehabilitation Hospital in Boston

the data collection, by checking the performance of the subject from different points of view, such as frontal and lateral. No excellent resolution performance is required for this type of camera for this purpose. An example of a normal camera is shown in figure 2.3.



Figure 2.3: Bonita Camera for VICON system

5. **Active Wand.** The optimization of the analysis volume influences the results in terms of precision and accuracy. To dynamically calibrate the cameras in the VICON motion capture space, both optical and video reference cameras, an active wand device is required (figure 2.4). It is composed by several active LED markers. "It enables you to achieve unparalleled accuracy with simultaneous multi-plane video calibration across an entire volume" [9]. Active

wands are designed to provide a spatial reference dimension that is precise and constant over time. They are normally designed to be insensitive to temperature and very rigid, so as not to undergo physical changes during calibration. On the wand, there is a label showing its factory length, with sub-millimeter precision. The average error accepted during calibration varies according to the volume to be framed, the number of positioned cameras and the purpose of the analysis. The key parameter, to define if the calibration has a good level, is the residual value. It is an offset distance between the different rays that converge during the reconstruction of a marker position. It is, therefore, an indicator of precision in the spatial reconstruction of a point. The lower the residual value, the greater the reconstruction precision, i.e. the rays agree more precisely, thus creating an accurate marker position. A well-traced point has an average sub-millimeter residual value. At the Spaulding Rehabilitation Hospital's Motion Analysis Lab, it was decided, for this project, to consider the calibration completed when the residual average value is less than or equal to 0.1.



Figure 2.4: Active Wand for VICON system [9]

This equipment, for both the laboratory and the subject, is necessary to record the performance of the patient under examination. After the positioning of both the infrared and standard cameras, the placement of the markers on the subject body, and the calibration of the system by shaking the active wand in the framed volume, the session can start, which lasts on average a couple of hours or more. After the data collection with the subject, additional time is needed to analyze the captured data by specialized personnel to obtain information on the subject's movements.

Necessary software and steps for data analysis

The software used to firstly process the captured data from the system is **Vicon Nexus** [10]. It has inherent pipelines and scripts to obtain the results from the VICON output [11].

The first step is the **Design of the marker set**. The information, that Vicon Nexus requires, is the explanation of how recognizing a subject, in particular, the joint and attached markers to track used during the data collection and the relationship between body segments, as the explanation of connected landmarks. To summarize, the software needs the structure of a labeling skeleton template. Once defined the set of markers to attach to the subject body, the structure always remains the same. Therefore, it is necessary to carry out this step only one time for each type of marker set used. When deciding on the positioning and the set of necessary markers, at least three markers per segment are needed (to be able to define a plane), and markers in the axes of the joints are necessary.

What must be done every time the subject changes is to define some parameters to be given to the software to calibrate the model. The information, such as the height of the subject, the length of the body segments, or the distance between the markers, must be measured before the session. Nexus is enabled to automatically label the skeleton during all the trials and to track the marker movements. To output valid kinematic or kinetic information, a predefined model can be used, such as Vicon Plug-in Gait, which involves running specific pipelines in Nexus, or an own made model by using Vicon BodyBuilder, MATLAB, or Python. The template contents provide the marker names, the skeletal structure, the marker set relationship, the joint type, etc. To obtain good results, a static trial is performed by the subject, to define the characteristics listed above. The position must be repeatable and it must be ensured that there are no marker occlusions and that only the subject under examination is present in the VICON volume. The results of subsequent analyses will depend on the quality of this step.

The second step is the **Creation of the subject node and preparation of the subject**. It involves the preparation, in the Data Management Lab, of a new and blank session for the subject. In this folder all the trials data are stored.

Capturing and reconstruction of the marker set is the next step. Positioned the subject in a base position, standing in a comfortable base pose, in the center of the capture volume, all the unlabeled markers must be shown in the 3D Perspective view. It is called the static trial.

In the subsequent step, **Addition of parameters to the labeling skeleton template**, the information of the physical measurements of the subject can be defined. It is not a mandatory step, but it can be a method to increase the accuracy of the future analysis.

In the **Creation of the skeletal structure** the reciprocal movement between markers is defined. In this way, the Vicon Nexus is enabled to automatically track the markers over time.

The Labeling Template Builder allow to move to the next phase, the **Creation of the skeletal segments**. The idea is to group the markers that move like in the same way, so the markers attached on the same body segment. A segment is

defined by three or more markers: one is the origin, one defines the primary axis of the segment and one defines the secondary axis. The figure 2.5 shows an example of the creation of the pelvis segments. It is possible to define different types of joints:

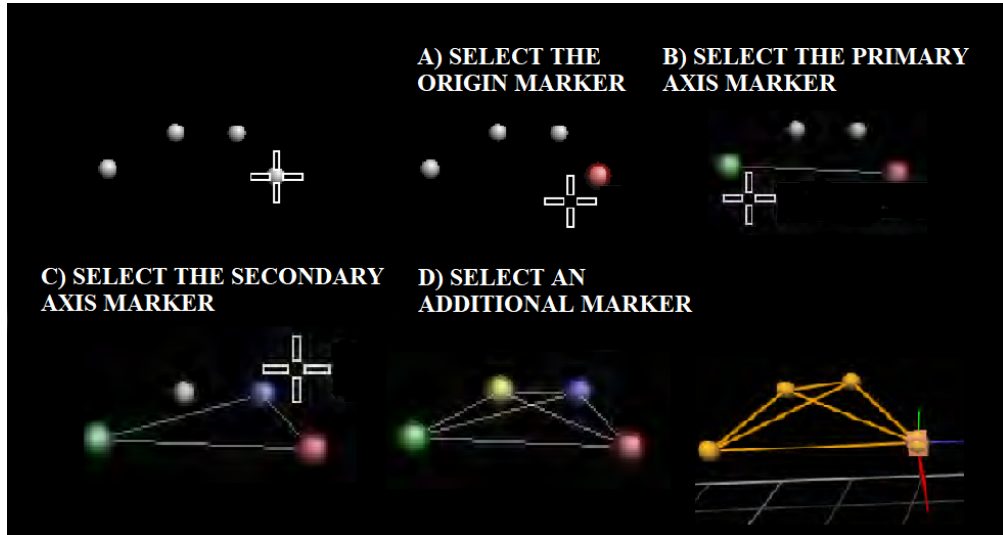


Figure 2.5: Creation of skeletal pelvis segments [11] (a) The first marker defines the location of one point (b) Two markers define a line (c) Three non co-linear markers define a plane (d) Four markers enable occluded markers to recreate the structure based on available markers

free Joint, for markers that can move freely independent of each other, ball Joint, for 3 DOF joint with full rotational freedom and not full translational freedom, hardy Spicer Joint, for 2 DOF joint with two rotational degrees, and hinge Joint, for only 1 DOF joint that allows rotation around one axis.

After this step, the **Assigning marker and segment properties** is possible, such as adding marker names, changing marker colors, etc.

Once the software has automatically labeled both the static and dynamic trials, in this case of the subject's walk, it is necessary to verify that it has been successful. It may happen that, due to unwanted reflections in the laboratory, some labels are missing in some frames of the trial. By manually checking the trajectories of the markers reconstructed over time, it is possible to identify these errors which present themselves as abrupt changes in the graph, which is most of the time due to swaps between marker labels. Once all the marker labels have been corrected in the various trials, the missing trajectories must be filled using the gap-filling technique, to have a smooth graph. There are different gap-filling methods: the spline fill, it consists of a cubic spline interpolation useful for short gaps, the rigid body fill, used for rigid or semi-rigid behavior amongst markers, pattern fill, it consists of applying the shape of another trajectory without gaps, cyclic fill, it

consists of looking the previous of later gait cycles, kinematic fill, it consists of considering how the markers are connected to the segment.

The last step is the use the **Plug-in Gait pipeline** to make the necessary kinematics and kinetics gait observations. after defining the position of the joint centers, shown in figure 2.6. The output is computed in the three anatomical planes: sagittal, frontal, and coronal. Despite the good quality of Vicon Nexus, it was decided to use a more robust software for the biomechanical analysis. The software used to process the data collected during the sessions and the trajectories obtain by the previous software is **Visual 3D**. Compared to Vicon Nexus, previously introduced, the program used is more robust in the analysis of the kinematics and kinetics of the gait. It is a Microsoft Windows application, that allows the use of pipelines already incorporated in the software, or it allows the use of own codes to extrapolate the information necessary for the study of the gait (figure 2.7). In this case, two models can be used for the reconstruction of the subject's skeleton, starting from the trajectories obtained with Vicon Nexus. The 6 DOF model, three rotational and three translational degrees, is the one traditionally used for gait analysis. It allows full freedom of movement at the joint points, without any restrictions. Mathematically the body segments are independent of each other. The inverse kinematics (IK) model instead allows you to constrain the movement of the segments concerning each other, not allowing full freedom of movement around the articular points.

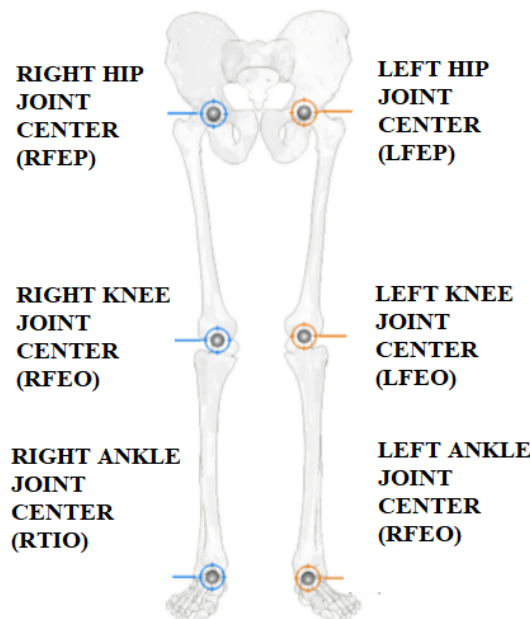


Figure 2.6: Vicon Nexus Joint centers position of the Plug-in Gait [12]

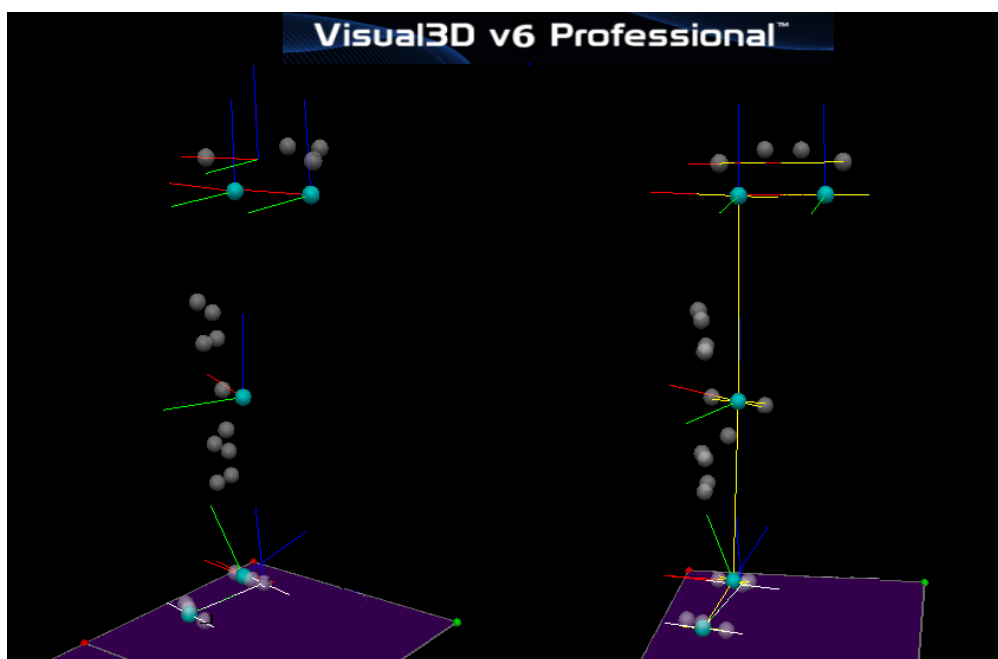


Figure 2.7: Visual 3D picture

2.2 OPENPOSE pose estimation tool

In this thesis work, a recent human 2D pose estimation tool, to detect the people present in the recorded videos of the subjects' walking sessions, is used. The choice fell on Openpose [13], among the many machine learning algorithms present in the field of computer science, as it is the first open-source and real-time system for pose estimation. This tool has the task of locating the anatomical parts of the people present in the videos provided, overcoming the limits and critical issues of the case: each video frame can contain an unknown number of human bodies that can present themselves in any position and scale; the interaction between the different subjects makes the association of the different body parts to the right person critical (for example, there may be occlusions or joints of the limbs).

There are numerous algorithms in this sector, which follow two possible approaches: the top-down approach, in which people in the image are firstly recognized and secondly the corresponding parts of the body are associated with these subjects considering both local observations, obtained through a convolutional neural network, and the spatial dependencies between them (the spatial relationships between adjacent parts of the body following a kinematic chain); the bottom-up approach, on the other hand, in which primarily parts of the body are recognized which, only later, are associated with an indefinite number of subjects in the image. The first approach takes advantage of single-person recognition at each iteration and

therefore suffers from the non-recovery of any errors previously committed, in addition, the computational time depends on the number of people in the image. The second approach, which is also used by Openpose, is characterized by good robustness and decouples this link between the time of the algorithm and the number of people. Openpose is "the first bottom-up representation of association scores via Part Affinity Fields, a set of 2D vector fields that encode the location and orientation of limbs over the image domain" [13]. The PAFs method, that "encodes unstructured pairwise relationships between body parts of a variable number of people" [13], guarantees this system high-quality results with a low computational time required by the algorithm.

Overall Pipeline

This paragraph presents the basic structure of the Openpose algorithm, as explained in the article [13]. As can be seen in figure 2.8, to obtain the 2D location of the anatomical points of each subject (*e*), the image to be analyzed is provided as an input to the algorithm (*a*). We define that this image has dimensions $[w \times h]$. Two successive feed forward steps are performed by the network to obtain the desired output:

- Initially, a series of 2D confidence maps of the locations of the body parts are predicted (*b* in figure 2.8). $\mathbf{S} = (\mathbf{S}_1, \mathbf{S}_2, \dots, \mathbf{S}_j)$, $\mathbf{S}_j \in \mathbb{R}^{w \times h}$ with $j \in \{1 \dots J\}$ and each j is a confidence map.
- Subsequently, a series of 2D vector fields of PAFs are predicted to encode the degrees of association between the previously predicted parts (*c* in figure 2.8). $\mathbf{L} = (\mathbf{L}_1, \mathbf{L}_2, \dots, \mathbf{L}_c)$, $\mathbf{L}_c \in \mathbb{R}^{w \times h \times x^2}$ with $c \in \{1 \dots C\}$ and each c is a vector field.

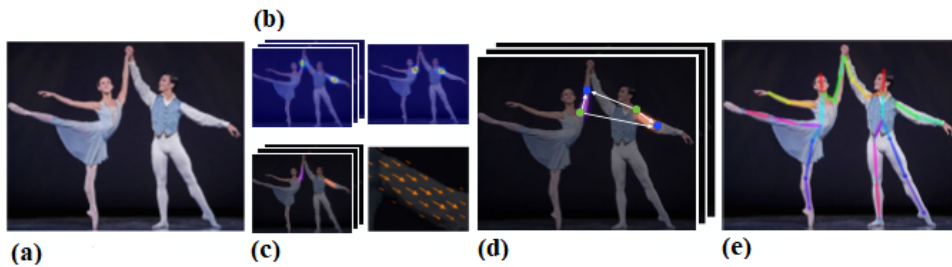


Figure 2.8: Openpose Pipeline [13]: (a) Input Image (b) Part Confidence Map (c) Part Affinity Fields (d) Bipartite Matching (e) Parsing Results

Network Architecture

The architecture [13] of the network is illustrated in figure 2.9. \mathbf{F} is the input of the first stage of the multi-stage CNN and it is composed of a set of feature maps obtained by providing the initial image to an analyzing CNN. As can be seen, the multi-stage network is then divided into two blocks. In the first part, PAFs are iteratively predicted which capture the different associations between different parts of the body present throughout the image. In the second part of the network, confidence maps are captured. The iterative method used allows improving any predictions in subsequent stages t , $t \in \{1 \dots T\}$, with an intermediate supervision step at each stage. In the current model, the network has three consecutive 3×3 kernels, with a total number of iterations equal to fifty-one, of which each output is concatenated to the next kernel. The steps of the network used, previously

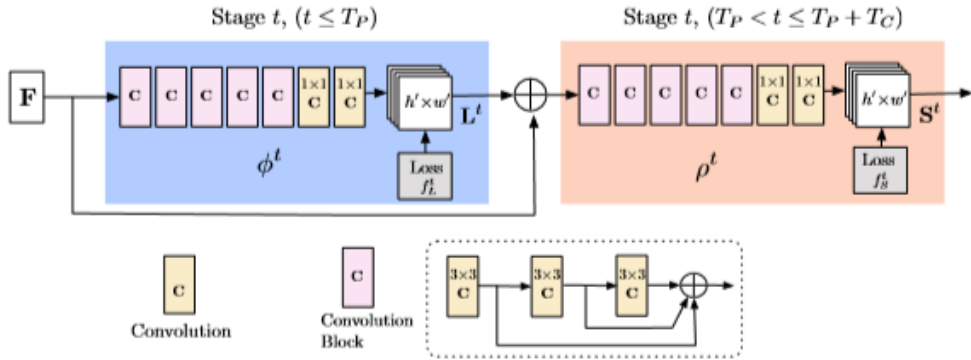


Figure 2.9: Openpose multi-stage Convolutional Neural Network Architecture [13]

introduced, are listed step by step:

1. The image is analyzed by a CNN and \mathbf{F} is generated, a set of feature maps, which will be provided at the first stage of the network;
2. In the first stage, the network takes \mathbf{F} as input and produces a set of PAFs. Then, in the subsequent stages, the original \mathbf{F} features of the image and the predictions of the previous stage are iteratively concatenated to refining the predictions (figure 2.10). The operation is repeated for the T_P iterations (the number of total PAFs stages).
3. Following the T_P iterations of the previous point, the process is repeated to obtain the confidence maps, starting from the most updated PAFs prediction, for a number of iterations equal to the total number of confidence map stages, T_C . The final confidence map is a 2D representation obtained starting from

the most updated PAFs predictions and it gives the idea that a certain part of the body is located in a certain pixel.

To guide the network in predicting PAFs of body parts (first block of the network) and confidence maps (second block of the network), a loss function is applied at the end of each stage. The loss function is spatially weighed to have a practical evaluation of the not-completely labeled people. Considering L_c^* as the ground truth PAFs, S_j^* as the ground truth part confidence map and $W(p) = 0$ where there is a missing annotation at the p-pixel, the equations used to calculate the loss functions in the different blocks are the following:

$$f_L^{t_i} = \sum_{c=1}^C \sum_p W(p) \cdot \|L_c^{t_i}(p) - L_c^*(p)\|_2^2, \quad (2.1)$$

$$f_S^{t_k} = \sum_{j=1}^J \sum_p W(p) \cdot \|S_j^{t_k}(p) - S_j^*(p)\|_2^2. \quad (2.2)$$

The overall equation is:

$$f = \sum_{t=1}^{T_p} f_L^t + \sum_{t=T_p+1}^{T_p+T_c} f_S^t. \quad (2.3)$$

Considering \mathbf{j} as the current body part, \mathbf{k} as the current detected person and $x_{j,k} \in \mathbb{R}^2$ the ground truth position, the value of the confidence maps at the \mathbf{p} -pixel location is defined as:

$$S_{j,k}^*(p) = \exp\left(-\frac{\|p - x_{j,k}\|_2^2}{\sigma^2}\right) \quad (2.4)$$

$$S_j^*(p) = \max_k S_{j,k}^*(p). \quad (2.5)$$

After detecting the different body parts, the parts association to the right people

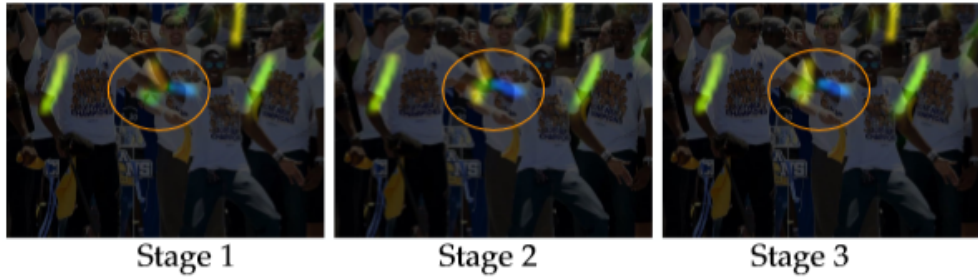


Figure 2.10: Example of Refinement of PAFs across stages [13]

and the full-bodies reconstruction are need. The PAFs method solves the problem

of creating false matches, preserving both the orientation and the location of the identified regions. "For each pixel in the area belonging to a particular limb, a 2D vector encodes the direction that points from one part of the limb to the other" [13]. Considering the image 2.11 in which \mathbf{c} is the considered limb and \mathbf{k} is considered

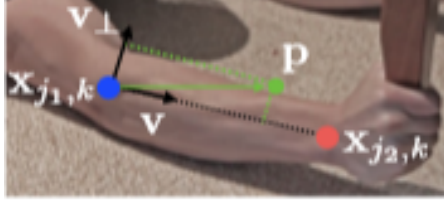


Figure 2.11: Part association [13]

the person, $x_{j_1, k}$ and $x_{j_2, k}$ are the ground truth positions of two different body parts, \mathbf{j}_1 and \mathbf{j}_2 . A unit vector is assigned to the \mathbf{p} -pixel depending on whether it belongs to the \mathbf{c} limb or not:

$$L_{c, k}^*(p) = \begin{cases} v = \frac{x_{j_2, k} - x_{j_1, k}}{\|x_{j_2, k} - x_{j_1, k}\|_2} & \text{if } p \text{ on limb } t, k \\ 0 & \text{otherwise} \end{cases} \quad (2.6)$$

The points that belong to the current \mathbf{c} limb are those within a certain distance from the line segment (from $x_{j_1, k}$ to $x_{j_2, k}$). Defining σ_1 the limb width in pixels and $l_{c, k} = \|x_{j_2, k} - x_{j_1, k}\|_2$ the \mathbf{c} limb length (used as a threshold), the limb points are defined as: $0 \leq v \cdot (p - x_{j_1, k}) \leq l_{c, k}$ and $\|v_\perp \cdot (p - x_{j_1, k})\| \leq \sigma_1$.

By averaging the affinity fields of the people detected, the PAF is defined as:

$$L_c^*(p) = \frac{1}{n_c(p)} \sum_k L_{c, k}^*(p) \quad (2.7)$$

where $n_c(p)$ are the non-zero vectors. "We measure the alignment of the predicted PAF with the candidate limb that would be formed by connecting the detected body parts" [13]. Defining \mathbf{d}_{j_1} and \mathbf{d}_{j_2} as candidate part locations, the line integration on the limb segment returns the association confidence between the two:

$$E = \int_{u=0}^{u=1} L_c(p(u)) \cdot \frac{d_{j_2} - d_{j_1}}{\|d_{j_2} - d_{j_1}\|_2} \partial u, \quad (2.8)$$

$$p(u) = (1 - u)d_{j_1} + ud_{j_2} \quad (2.9)$$

where $\mathbf{p}(\mathbf{u})$ is the interpolation of the two candidates.

Once all the parts of the body present in the image have been identified, the parts belonging to the same limb must be associated, i.e. create the limb pairs between the

possible connections, and then associate the connected limbs obtained to the right person among the various possible candidates. With the previous equation 2.8, first of all, a weight is given to the edges of all the possible connections between the parts; therefore a K -matching problem must be solved to find the optimal correspondences. Defining \mathbf{N}_j the amount of body part candidates for a certain part \mathbf{j} , $d_j^m \in \mathbb{R}^2$ the location of the \mathbf{m} -th candidate, $D_j = \{d_j^m : for j \in \{1 \cdots J\}, m \in \{1 \cdots N_j\}\}$ is the set of those possible body parts. To find the connection between the previous body parts, the variable $z_{j_1 j_2}^{mn} \in \{0,1\}$ indicate the connection between two of those candidates, $d_{j_1}^m$ and $d_{j_2}^n$. The final aim is to assign optimally the connections between the different body parts, considering the set of all the possibility as $Z = \{z_{j_1 j_2}^{mn} : for j_1, j_2 \in \{1 \cdots J\}, m \in \{1 \cdots N_{j_1}\}, n \in \{1 \cdots N_{j_2}\}\}$. All the weighted edges are possible connections and by resolving a maximum weight bipartite graph matching problem the associations can be defined:

$$\max_{Z_c} E_c = \max_{Z_c} \sum_{m \in D_{j_1}} \sum_{n \in D_{j_2}} E_{mn} \cdot z_{j_1 j_2}^{mn}, \quad (2.10)$$

where \mathbf{E}_c is the overall weight for limb \mathbf{c} , \mathbf{Z}_c is the subset of \mathbf{Z} for \mathbf{c} and \mathbf{E}_{mn} is the part affinity between $d_{j_1}^m$ and $d_{j_2}^n$.

Two constraints are used to be sure that no a node is shared by two edges 2.11 and no a part is shared by two of the same type limbs 2.12:

$$\forall m \in D_{j_1}, \sum_{n \in D_{j_2}} z_{j_1 j_2}^{mn} \leq 1, \quad (2.11)$$

$$\forall n \in D_{j_2}, \sum_{m \in D_{j_1}} z_{j_1 j_2}^{mn} \leq 1. \quad (2.12)$$

In addition, for the Openpose algorithm, two more relations are added to solve the matching problem. In particular, firstly a minimum number of edges is chosen to obtain a tree skeleton, and secondly, the problem is divided into bipartite independently matching problems ((d) in figure 2.12) because of the use of PAFs method, for adjacent tree nodes, and the CNN, for not adjacent nodes. The final optimization is given by the equation:

$$\max_Z E = \sum_{c=1}^C \max_{Z_c} E_c. \quad (2.13)$$

A brief guide on the use of the Openpose tool is provided in the appendix A. The necessary characteristics of the work machine in which to use it and a practical description of the system output are described.

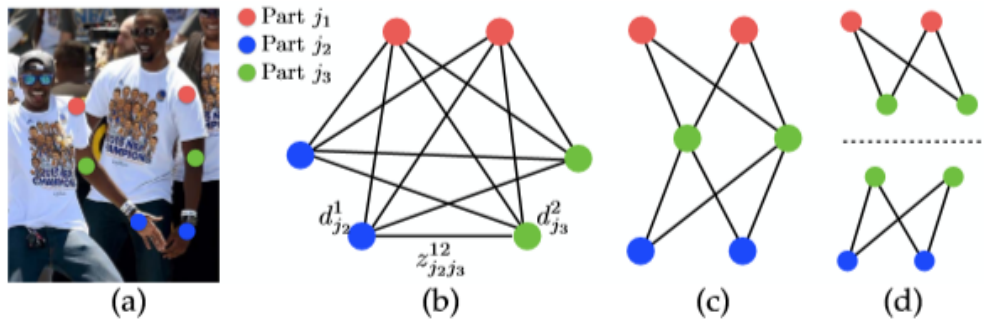


Figure 2.12: Graph matching [13]: (a) Part detection (b) K-graph (c) Tree structure (d) Bipartite graph

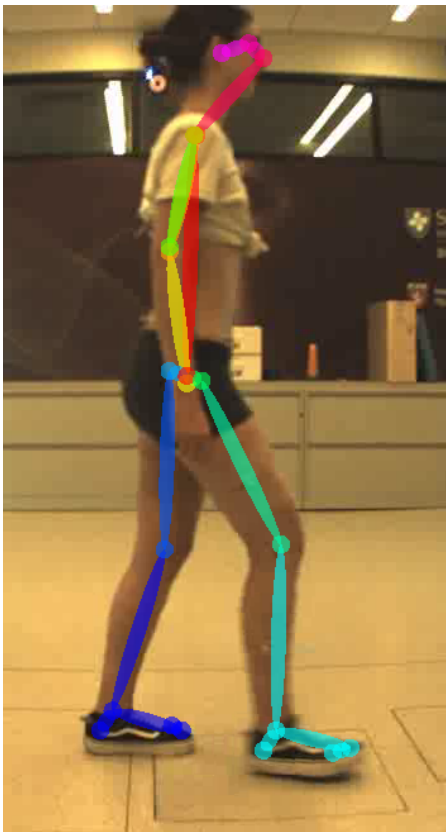


Figure 2.13: An example of the Openpose Output from a lateral view of the subject

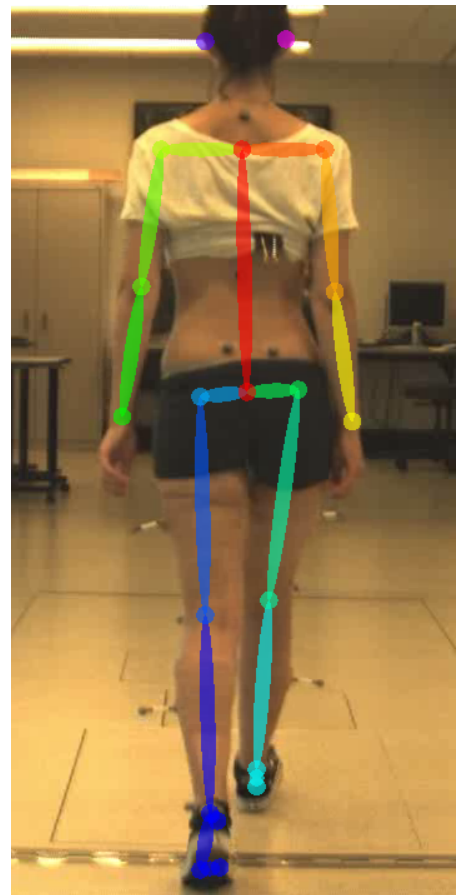


Figure 2.14: An example of the Openpose Output from a frontal view of the subject

Chapter 3

Materials and Methods

3.1 Protocol and Procedures

In this chapter, the used protocol and procedures for the data collection are described. The data collection and the data analysis took place in the Motion Analysis Lab at Spaulding Rehabilitation Hospital in Boston.

Five healthy subjects, with no motor impairments, three males and two females, with a mean age equal to 27 ± 7 , were recruited for the preliminary analysis. Table 3.1 shows the demographic information of the chosen subjects.

Table 3.1: General information on the recruited subjects

Subject	Gender	Age	Weight (kg)	Height (m)
1	F	25	52	1.67
2	M	26	65	1.80
3	F	25	78	1.69
4	M	24	62	1.71
5	M	34	83	1.83

First, the VICON system was turned on and the position of the infrared cameras was checked. The treadmill used during the data collection, to have a walk that is as repeatable as possible and in a fixed position in respect to the cameras, is positioned in the middle of the laboratory at the center of the VICON volume. The Bonita cameras, the two additional standard cameras used to validate the performance of the subject and to record videos for the Openpose tool, are placed in the lateral and frontal positions in respect to the treadmill. Two passive markers are placed on the treadmill, one in the front part and one in the back part concerning the sliding carpet, to have a reference of the treadmill length.

The system is then calibrated, by shaking the active wand in the desired volume. To prepare the subject, nineteen retro-reflective markers are attached on the body in certain key-points of the right lower limb.

The chosen marker-set is composed by:

- 4 markers positioned on the pelvis: the left and right anterior-superior iliac, and the left and right posterior-superior iliac;
- 2 markers positioned on the lateral and medial knee epicondyles;
- 2 markers positioned on the lateral and medial ankle malleoli;
- 3 markers positioned on the foot: the heel, the 5th metatarsal head, and the 1st metatarsal head, attached on the subject shoes;
- 4 markers positioned on the thigh (forming a square);
- 4 markers positioned on the shank (forming a square).

At the beginning of the experiment, for each subject, the self-selected walking speed on the treadmill was defined, by ascending from 0 km h⁻¹, to find the first estimate, by descending subsequently from 1.5· the first estimate to find the second estimate, and at last by averaging the two estimates and by choosing the speed closest to 3.6 km h⁻¹ (1.0 m s⁻¹), 4.0 km h⁻¹ (1.1 m s⁻¹), 4.4 km h⁻¹ (1.2 m s⁻¹), etc. At a later time, being the self-selected speeds very similar for all the subjects, it was chosen to use the same speed for all subjects, to also have comparable walks:

Table 3.2: Walking speeds for the treadmill sessions

Session	Speed (km h ⁻¹)	Speed (m s ⁻¹)
Normal walk	4.0	1.1
Fast walk	6.0	1.7
Slow walk	2.0	0.6

Defined the walking speeds, the data collection can start.

Two kinds of trials must be performed.

The first one is the static trial, in which the subject stands on the treadmill in a base comfort position, to allow the definition of the body segments length on the picture, the reference joint angles and to calibrate the retro-reflective markers for the VICON system.

The second trial consists of the walking sessions, that last two minutes each, performed 6 times at the three randomized speed walks, two walks for each speed (in table 3.2).

During the whole data collection, the subject is recorded by the VICON cameras, that capture the reflective light of the passive markers, and the standard cameras, that records the session from the lateral and frontal points of view.

Two steps are needed later to extract the necessary data for the gait analysis:

1. The VICON data are obtained by using both the software, VICON Nexus and Visual 3D, to reconstruct the body skeleton of the subject starting from the markers position and to extract the gait data from the markers trajectory (VICON data);
2. The video recordings from the standard cameras are provided to the Openpose tool to obtain the body key-points of the subjects, predicted by the CNN. The OPENPOSE data are obtained by processing the data in Matlab [14].

An additional step is necessary to adequately carry out the analysis of the OPENPOSE data collected. Starting from the standard cameras, the Bonita cameras in this project, the rectification of the video-frames is necessary to have not distorted pictures, so a better prediction of the joints. For this reason, the last step of the data collection is an additional video recording, by moving a chessboard in front of the two standard cameras, to provide information to the Matlab "Camera Calibration" tool to define the lenses parameters (Appendix B).

3.2 Data analysis

Starting from the data provided by the VICON system and the OPENPOSE tool, the thesis work aims to carry out a preliminary analysis of the gait to subsequently comparing the two results and define whether the pose estimation tool can be reliable for gait analysis.

The main objectives of the work are the comparison of the two biomechanical models, in terms of body segments-orientation and joint-angles, the comparison of the position of the centers of rotation estimated by the systems and the characterization of the OPENPOSE estimated error in terms of angles shape, angles magnitude and markers displacement.

3.2.1 Rectification of the video recordings

The first step of the data processing is the rectification of the frames that compose the videos, recorded by the Bonita cameras, during the walking sessions.

The Matlab tool [15], called **camera calibrator**, is used primarily to estimate the parameters of the lenses of the cameras. The functioning of the Matlab library is briefly explained below, and a guide on its use is provided in the appendix B.

The camera calibrator, also referred to as "camera resector", is a tool provided by Matlab to estimate the geometric parameters, both intrinsic and extrinsic, and lens distortion parameters of a single camera (figure 3.1).

First, it is important to know the points of the 3D world and the corresponding 2D points of the image, as shown in figure 3.2. It was decided to use a checkerboard as a calibration tool to obtain the aforementioned matches.

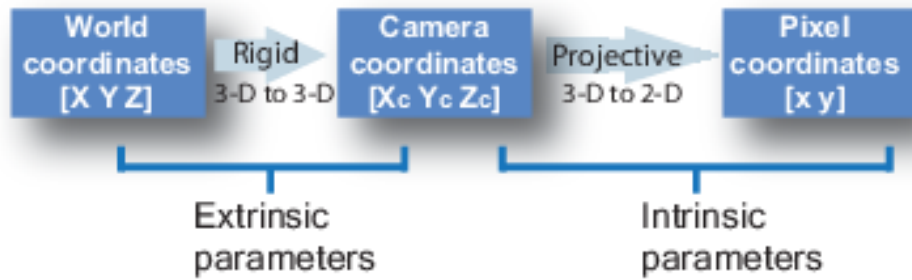


Figure 3.1: Definition of the role of extrinsic and intrinsic parameters [15]

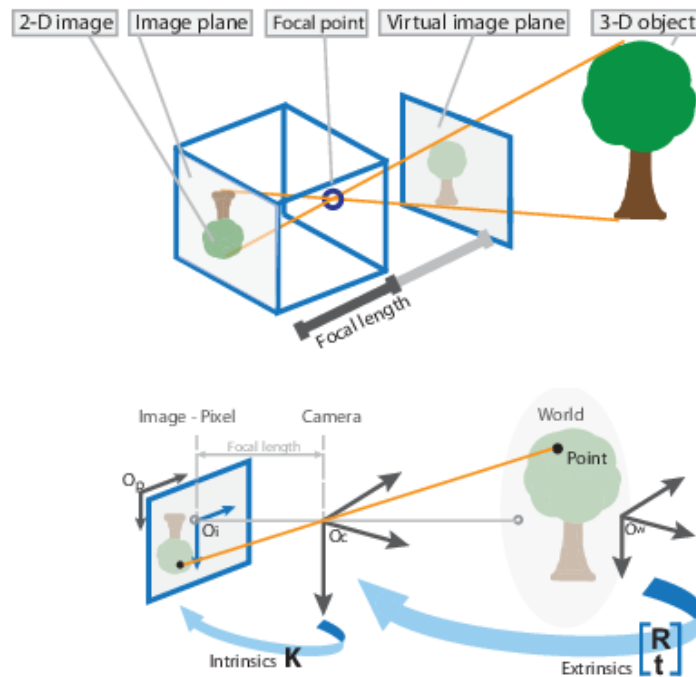


Figure 3.2: Illustration of how a camera works [15]

The calibrator can define:

- The extrinsic parameters that represent the rigid transformation from the 3D coordinate system of the world to the 3D coordinate system of the camera, which origin is located at the optical center of the camera, and its x-axis and y-axis define the picture plane. These parameters consist of a rotation \mathbf{R} , and a translation \mathbf{t} (figure 3.3).
- The intrinsic parameters represent a projective transformation from the 3D coordinates of the camera to the 2D coordinates of the image. These parameters consist of the focal length (figure 3.2), the optical center that is the principal point, and the skew coefficient (figure 3.4).

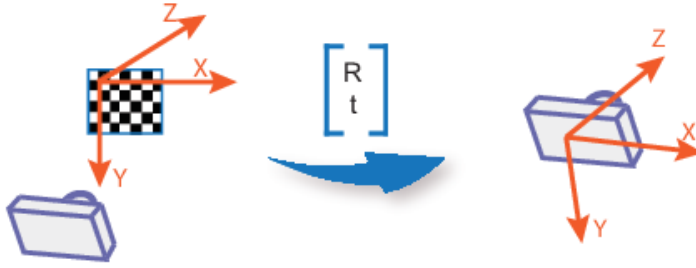


Figure 3.3: Extrinsic parameters of the camera [15]

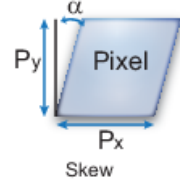


Figure 3.4: Pixel skew definition [15]

Knowing the points of the image and the world, thanks to the use of the chessboard,

the following relations hold: $w[xy1] = [XYZ1] \cdot P$, $P = \begin{bmatrix} R \\ t \end{bmatrix} \cdot K$, $K = \begin{bmatrix} f_x & 0 & 0 \\ s & f_y & 0 \\ c_x & c_y & 1 \end{bmatrix}$,

$s = f_x \cdot \tan \alpha$; where \mathbf{w} is the scale factor, \mathbf{x} and \mathbf{y} are the image points, \mathbf{X} , \mathbf{Y} , \mathbf{Z} are the world points, \mathbf{P} is the camera matrix, \mathbf{R} and \mathbf{t} contain the extrinsic rotation and translation, \mathbf{K} contains the intrinsic parameters, \mathbf{c}_x and \mathbf{c}_y define the optical center in pixels, \mathbf{f}_x and \mathbf{f}_y define the focal length in pixels, s is the skew coefficient and α is defined in figure 3.4.

The image distortion can be both radial (figure 3.5) and tangential (figure 3.6). The first one is defined by the equations $x_{distorted} = x(1 + k_1 \cdot r^2 + k_2 \cdot r^4 + k_3 \cdot r^6)$ and $y_{distorted} = y(1 + k_1 \cdot r^2 + k_2 \cdot r^4 + k_3 \cdot r^6)$; where \mathbf{x} and \mathbf{y} are the undistorted pixel locations and \mathbf{r} are the radial distortion coefficients of the lens. The second one is defined by the equations $x_{distorted} = x + [2 \cdot p_1 \cdot x \cdot y + p_2 \cdot (r^2 + 2 \cdot x^2)]$ and $y_{distorted} = y + [p_1 \cdot (r^2 + 2 \cdot y^2) + 2 \cdot p_2 \cdot x \cdot y]$; where \mathbf{x} and \mathbf{y} are the undistorted pixel locations and \mathbf{p} are the tangential distortion coefficients of the lens.

First of all, in this project, 43 images were provided at the input of the calibrator, in which the checkerboard was present in different points of the space. The size

RADIAL DISTORTIONS IN PICTURES

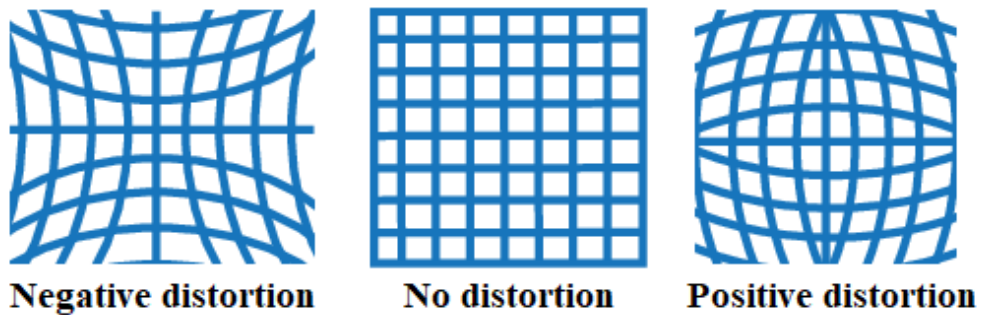


Figure 3.5: Types of radial distortion in pictures [15]

TANGENTIAL DISTORTION IN PICTURES

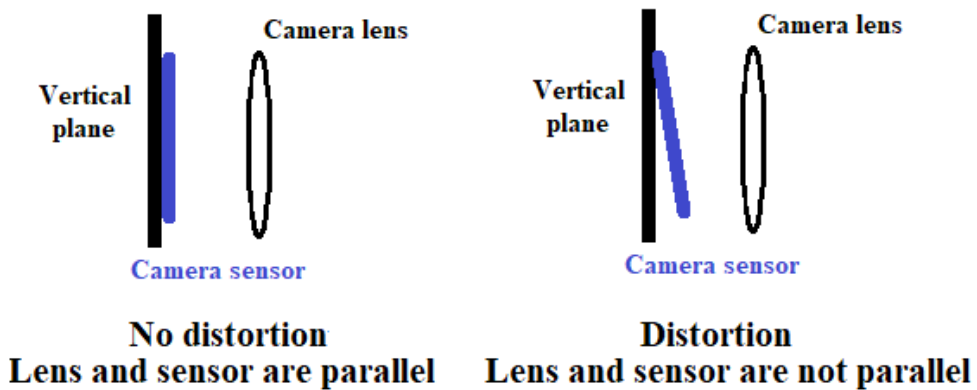


Figure 3.6: Types of tangential distortion in pictures

of the used chessboard square was 23 mm. The tool was able to recognize the checkerboard in the pictures and it returned the parameters of the lenses, that were used in a second time to rectify all the recorded videos. In table 3.3 the calculated lenses parameters of the used standard cameras are provided. Using the output of the Matlab tool for the calibration of the cameras, which is a structure containing all the lens parameters (table 3.3), it is possible to rectify all the frames of the recorded videos. The rectified pictures are then provided as input to the Openpose tool for predicting key points of the body, frame by frame. In figure 3.7 the same image is shown. The image above is one of the uploaded figures in the Matlab tool, that is processed by the camera calibrator. The checkerboard is recognized and the lens parameters are exported. The below image represents the same scene, that is rectified using the parameters provided by the tool.

Table 3.3: Lenses parameters of the Bonita cameras

Image Size	[720, 1280]
Radial Distortion	[-0.0494, 0.0017]
Tangential Distortion	[0, 0]
World Points	54x2 double
World Units	mm
Principal Point	[634.7126, 359.8283]
Num Patterns	43
Intrinsic Matrix	[336.8044,0,0; 0,334.2413,0; 634.7126,359.8283,1]
Focal Length	[336.8044, 334.2413]
Skew	0
Rotation Vectors	43x3 double
Translational Vectors	43x3 double
Reprojected Points	54x3x43 double
Mean Reprojection error	0.1916
Rotation Matrices	3x3x43 double

3.2.2 Definition of the scale factor to convert meter to pixel

The first problem to be addressed is the definition of the scale factor which allows obtaining the data of both systems, VICON and OPENPOSE, in the same unit of measurement. The VICON system returns the position of the markers over time using the **meter** as the unit of measure. On the other hand, OPENPOSE works with pictures, so the coordinates of the predicted landmarks are returned in **pixel**. To address the problem, two passive markers were placed on the treadmill during the data collection (figure 3.8). By using the VICON system it is possible to obtain the coordinates of the two markers, in respect to the VICON reference system. To have the coordinates in pixel of the same markers in the pictures, it is used the Matlab **ginput** function, that allows to point with the mouse the markers of interest. Considering the marker placed in the back part of the treadmill as \mathbf{P}_1 , and the marker placed in the front part as \mathbf{P}_2 , (x', y', z') the coordinates in the VICON reference system, (x'', y'') the coordinates in the OPENPOSE reference system, the tables 3.4 and 3.5 show the treadmill coordinates for all the five subjects. Considering the appropriate axes for the two systems, the length of the treadmill \mathbf{L} is computed as:

$$L_m = \|\mathbf{P}_1(y') - \mathbf{P}_2(y'), \mathbf{P}_1(z') - \mathbf{P}_2(z')\|; \quad (3.1)$$

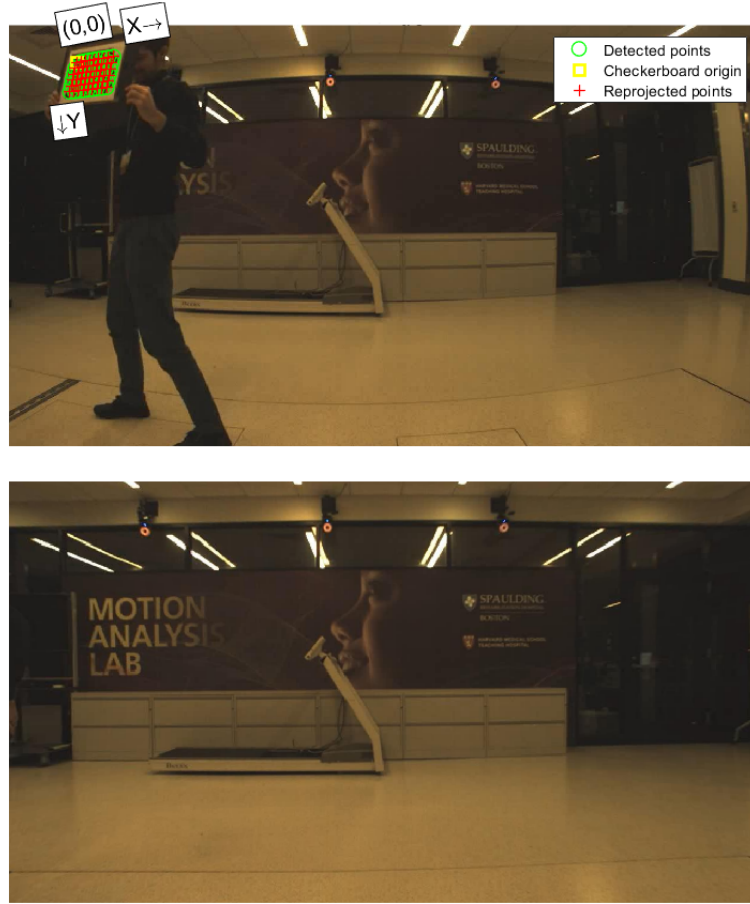


Figure 3.7: Pictures, both distorted and undistorted, of the Motion Analysis Lab at Spaulding Rehabilitation Hospital in Boston

$$L_{pixel} = \|P_1(x'') - P_2(x''), P_1(y'') - P_2(y'')\|. \quad (3.2)$$

Knowing the length of the treadmill in the two units of measurement (table 3.6), we define the scale factor f , to convert the length from meters to corresponding pixels in the image as follows in the equation 3.3.

$$f = \frac{L_{pixel}}{L_m}. \quad (3.3)$$

Table 3.4: Treadmill markers position for subject 1, 2, and 3

	Subject 1	Subject 2	Subject 3
$P_1 (x', y', z')$	[0.4091, 1.6641, 0.1530]	[0.4224, 1.5235, 0.1476]	[0.4224, 1.5236, 0.1477]
$P_2 (x', y', z')$	[0.4127, 0.0658, 0.1572]	[0.4481, -0.0766, 0.1569]	[0.4483, -0.0765, 0.1561]
$P_1 (x'', y'')$	[417.7500, 563.7500]	[311.2500, 596.7500]	[311.2500, 596.7500]
$P_2 (x'', y'')$	[915.7500, 560.7500]	[867.7500, 584.7500]	[869.2500, 586.2500]

Table 3.5: Treadmill markers position for subject 4, and 5

	Subject 4	Subject 5
$P_1 (x', y', z')$	[0.4248, 1.5236, 0.1485]	[0.4224, 1.5236, 0.1477]
$P_2 (x', y', z')$	[0.4462, -0.0765, 0.1569]	[0.4483, -0.0765, 0.1561]
$P_1 (x'', y'')$	[311.2500, 598.2500]	[311.2500, 596.7500]
$P_2 (x'', y'')$	[869.2500, 584.7500]	[869.2500, 586.2500]

3.2.3 Definition of the new reference system

As shown above, the two systems in comparison use two different reference systems. For this reason, it is necessary to identify a common point that could become the origin of a new reference system common to the two systems. It was chosen to use the marker positioned in the front part of the treadmill, \mathbf{P}_2 , as the origin of the new axes, and all coordinates of the markers attached on the subject's body are scaled accordingly.

Considering \mathbf{P}_r a certain point, (x, y) the coordinates considering the new axes for both the systems, (x', y', z') the coordinates considering the VICON axes, (x'', y'') the coordinates considering the OPENPOSE axes and the lateral point of view, and (z'') the coordinate considering the OPENPOSE axis and the frontal point of view,

$$\begin{cases} P_r(x) = P_r(y') - \Delta y' \\ P_r(y) = P_r(z') - \Delta z' \\ P_r(z) = P_r(x') - \Delta x' \end{cases} \quad (3.4)$$

$$\begin{cases} P_r(x) = -(P_r(x'') - \Delta x'') \\ P_r(y) = -(P_r(y'') - \Delta y'') \\ P_r(z) = -(P_r(z'') - \Delta z'') \end{cases} \quad (3.5)$$

$\Delta x', \Delta y', \Delta z'$ mean the distance, along the three axes (x', y', z') , of the marker P_2 , the origin of the new reference system, with the origin of the VICON reference system. $\Delta x'', \Delta y'', \Delta z''$ mean the distance of the marker P_2 , the origin of the new

Table 3.6: Treadmill length (both in meter and pixel), and scale factor values computed for the five subjects

	Subject 1	Subject 2	Subject 3	Subject 4	Subject 5
L (m)	1.5983	1.6001	1.6001	1.6001	1.6001
L (pixel)	498	556	558	558	558
f	311.5770	347.7859	348.7328	348.7328	348.7328

reference system, with the origin of the OPENPOSE reference system; $\Delta x''$, $\Delta y''$ refers the distance along the two axes (x'' , y'') considering the lateral view, $\Delta z''$ refers the distance along the two axes (z'') considering the frontal view.

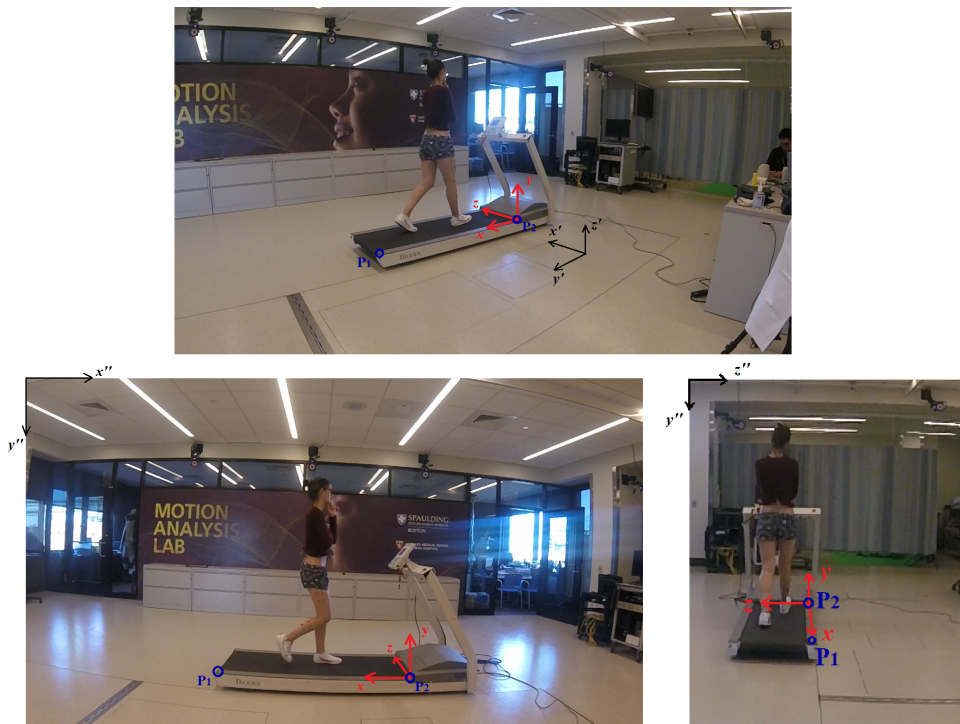


Figure 3.8: Illustration of both the reference systems, above for the VICON system, and below for the OPENPOSE pictures. In red the new reference system used and in blue the position of the markers placed on the treadmill

3.2.4 Processing of OPENPOSE trajectory signals

Once provided to the OPENPOSE tool all the frames that compose the videos recorded during the walking sessions of the subject under examination, it returns, frame by frame, the coordinates of the key-points of the body. Once the problem of the reference system has been addressed, the trajectories over time of each landmark for each walking session are known.

The raw data appear very noisy, and as can be seen in the graphs 3.9 and 3.10, there is a swaying background noise probably due to the continuous oscillations over time of the same landmark in the frames.

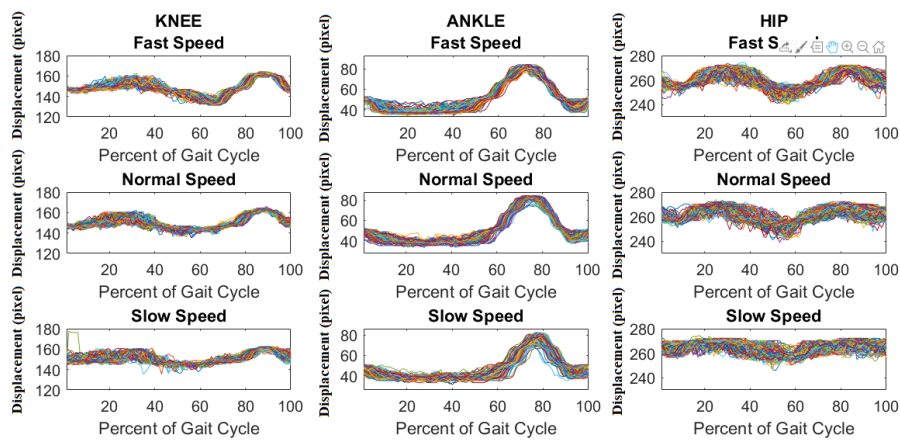


Figure 3.9: Raw trajectories, step by step, of the y-coordinate of the leg joints: hip, knee, and ankle (subject 1)

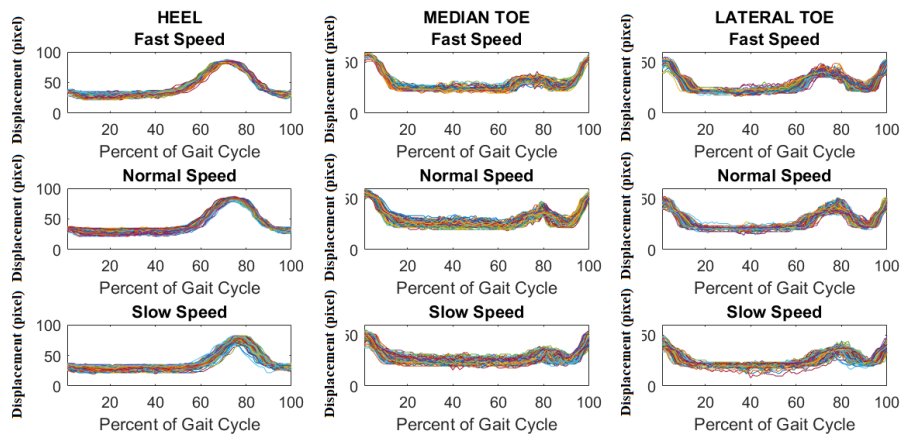


Figure 3.10: Raw trajectories, step by step, of the y-coordinate of the foot joints: heel, median toe, and lateral toe (subject 1)

Furthermore, in some frames, the pose estimation tool is not able to correctly position the joint of the body, thus assigning it a null value (in the old reference system). To solve these problems, two types of filters have been adopted to obtain cleaner and clearer signals.

Initially, a **median filter** is adopted to remove the outliers, those peaks that appear in the signal due to failure recognition of the position of the joint in that frame. It happens that the joint is not recognized in a variable number of subsequent frames, for this reason, different orders of the smoothing filter were tried and the chosen order changes subject by subject (table 3.7). The Matlab function used is *medfilt1*. Considering n the chosen order of the median filter and an odd value, the function returns the median value as $y(k) = x(k - (n - 1)/2 : k + (n - 1)/2)$.

The second filter used is a low-pass filter, to delete the noisy components of the raw signal. To avoid the ripple in both the pass and stop band, and to guarantee a high slope at the cutoff frequency (figure 3.11), the **Chebyshev filter of type 1** is chosen. The squared form of the frequency response in this class of filter, considering N the order of the filter, $\omega_p = 2\pi f_p$ the pulsation that defines the bandwidth, ϵ the bandwidth oscillation factor and $T_N(x)$ the Chebyshev polynomial of order N :

$$\|H_a(j\omega)\|^2 = \frac{1}{1 + \epsilon^2 T_N\left(\frac{\omega}{\omega_p}\right)^2}, \quad (3.6)$$

$$T_N\left(\frac{\omega}{\omega_p}\right) = \begin{cases} \cos N \arccos\left(\frac{\omega}{\omega_p}\right), & 0 \leq \frac{\omega}{\omega_p} \leq 1 \\ \cosh N \cosh^{-1}\left(\frac{\omega}{\omega_p}\right), & 0 \leq \frac{\omega}{\omega_p} \leq \inf \end{cases} \quad (3.7)$$

To find the correct cut-off frequency for each subject (table 3.7), the residual analysis is performed, that is the difference between the filtered signal and the original one. As could be seen in figure 3.13, the spectrum of the residue is a flat curve, which indicates the whiteness of the noise. The signal spectrum estimate was calculated using the Schuster periodogram.

Figure 3.14 shows the result of the filter applied to a random trajectory signal. It was chosen to use an anti-causal filter to avoid the phase distortion, that is computed by the Matlab *filtfilt* function.

Table 3.7: Values of the window length used for the median filter, and cut-off frequencies of the low-pass filter

	Subject 1	Subject 2	Subject 3	Subject 4	Subject 5
Median filter order	5	5	11	11	11
Cutoff frequency (Hz)	15	15	15	15	15

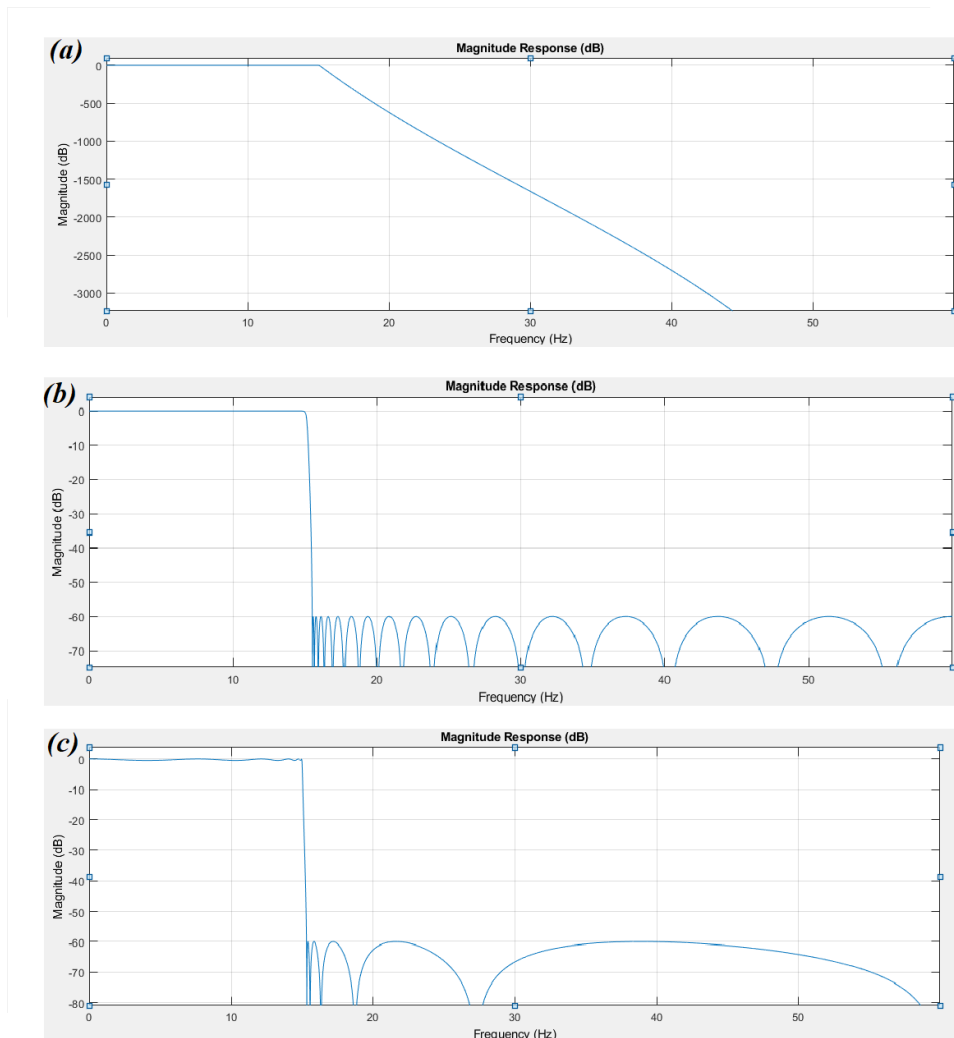


Figure 3.11: Masks of the three different filters (a) Butterworth (b) Chebyshev (c) Elliptic

3.2.5 Extraction of angles from the position of the key-points

Starting from the coordinates of the frame by frame key-points, provided by the Openpose tool, it is possible to calculate the angles of the main joints of the subject's leg. For the analysis to be carried out, three angles are necessary for the evaluation of the subject gait: the hip angle, the knee angle and the ankle angle. Figure 3.17 shows the biomechanical definition of the previous angles considering the sagittal plane.

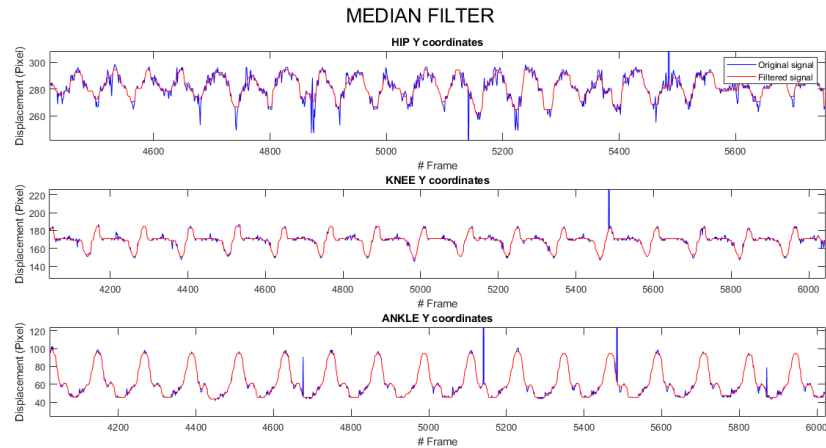


Figure 3.12: Effect of the median filter on the original signal. It shows the trajectory of the hip, knee, and ankle coordinate of subject 1 during fast walk (subject 1)

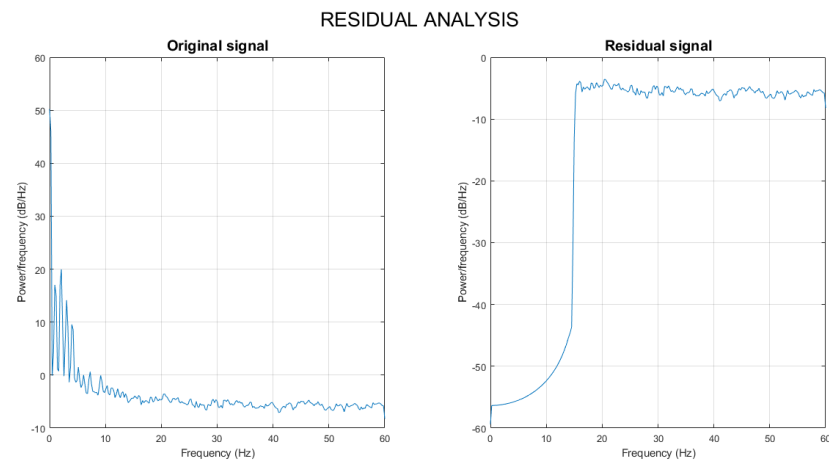


Figure 3.13: Residual analysis of a trajectory signal to find the correct cutoff frequency (subject 1)

From the biomechanical point of view, the **hip angle** is defined as the angle between the axis of the pelvis and the axis of the femur. This angle is considered positive in case of hip flexion, and negative in case of hip extension. Not having the pelvis axis available starting from the two-dimensional pictures from the lateral point of view, it was decided to use a straight line perpendicular to the subject's trunk axis (figure 3.18).

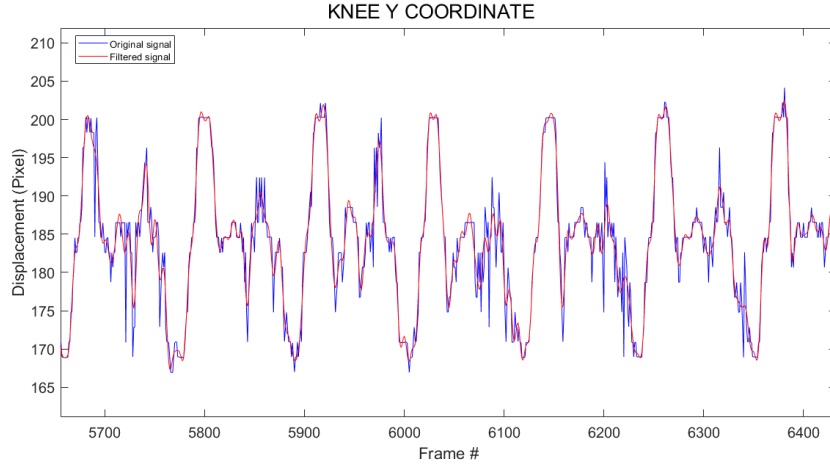


Figure 3.14: Result of the Chebyshev filter applied on the trajectory signal (subject 1)

Firstly the trunk segment and the femoral segment are defined by using the equations:

$$\begin{cases} m = \frac{y_2 - y_1}{x_2 - x_1} \\ k = y_1 - m \cdot x_1 \end{cases} \quad (3.8)$$

Considering the trunk segment, (x_1, y_1) are the current coordinates of the neck, (x_2, y_2) are the current coordinates of the pelvis center. By using the previous equations 3.8 the angular coefficient is \mathbf{m}_1 , that quantifies the slope of the straight line, and the known term is \mathbf{k}_1 , that indicates the point where the straight line intercepts the y-axis. The straight line perpendicular to the trunk axis has the angular coefficient defined as $m_1 \perp = -\frac{1}{m_1}$.

In the same way, considering the femoral segment, (x_1, y_1) are the current coordinates of the hip, and (x_2, y_2) are the current coordinates of the knee. By using the previous equations 3.8 the angular coefficient is \mathbf{m}_2 , and the known term is \mathbf{k}_2 . The angle formed by the two previous straight lines, the trunk and the femur, is defined:

$$\alpha = 90 - \arctan \left\| \frac{m_1 \perp - m_2}{1 + m_1 \perp \cdot m_2} \right\| \cdot \frac{360}{2 \cdot \pi}. \quad (3.9)$$

Considering two half-planes formed by the straight lines, the sign of the angle is defined according to the position of the knee joint, or the belonging of the knee to one of the half-planes.

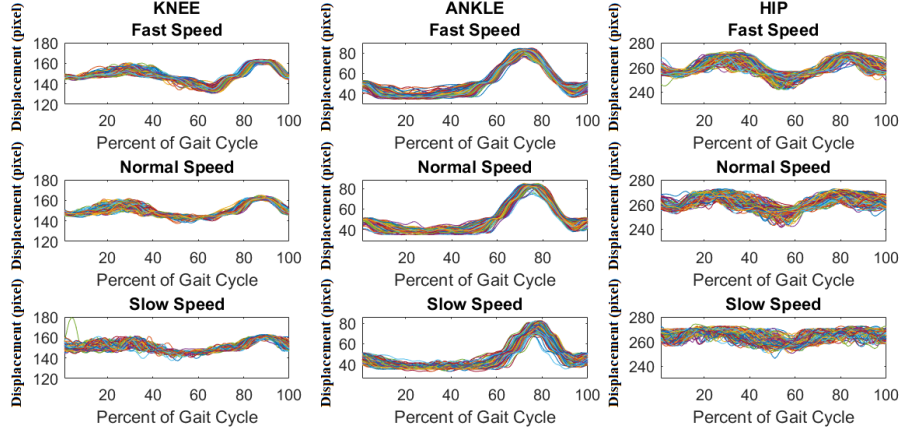


Figure 3.15: Filtered trajectories, step by step, of the y-coordinate of the leg joints: hip, knee, and ankle (subject 1)

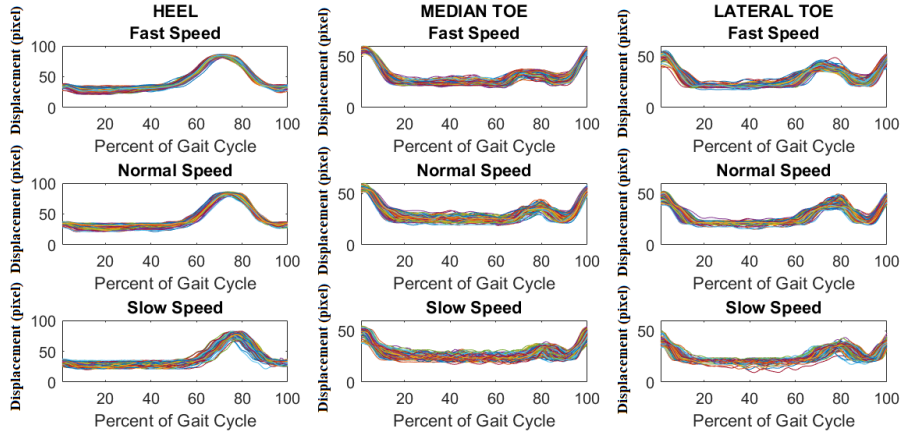


Figure 3.16: Filtered trajectories, step by step, of the y-coordinate of the foot joints: heel, median toe, and lateral toe (subject 1)

The **knee angle** is defined as the angle between the axis of the femur and the axis of the tibia. This angle is considered positive in case of knee flexion, and negative in case of knee extension. The femur segment and the tibia segment are defined by using the equations 3.8. Considering the femoral segment, (x_1, y_1) are the current coordinates of the hip, and (x_2, y_2) are the current coordinates of the knee. By using the previous equations 3.8 the angular coefficient is \mathbf{m}_1 , and the known term is \mathbf{k}_1 . For the tibial segment, (x_1, y_1) are the current coordinates of the knee, and (x_2, y_2) are the current coordinates of the ankle. By using the previous equations 3.8 the angular coefficient is \mathbf{m}_2 , and the known term is \mathbf{k}_2 .

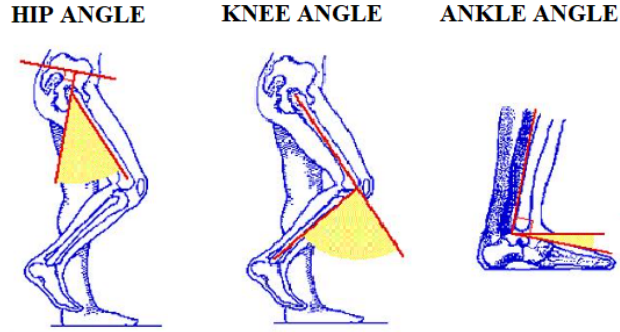


Figure 3.17: Bio mechanical definition of the hip, knee, and ankle angles

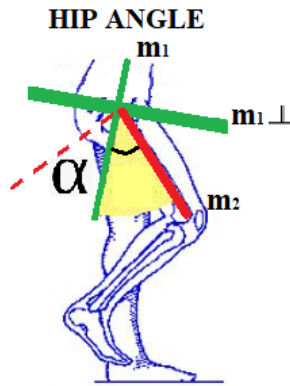


Figure 3.18: Definition of the hip angle

The angle formed by the two previous straight lines, the femur and the tibia, is defined:

$$\alpha = \arctan \left\| \frac{m_1 \perp - m_2}{1 + m_1 \perp \cdot m_2} \right\| \cdot \frac{360}{2 \cdot \pi}. \quad (3.10)$$

Also for the knee angle it is possible considering two half-planes formed by the straight lines, and the sign of the angle is defined according to the position of the ankle joint, or the belonging of the ankle to one of the half-planes.

The **ankle angle** is defined as the angle between the axis of the tibia and the axis of the foot. This angle is considered positive in case of plantar-flexion, and negative in case of dorsi-flexion. The tibia segment and the foot segment are defined by using the equations 3.8. Considering the tibia segment, (x_1, y_1) are the current coordinates of the knee, and (x_2, y_2) are the current coordinates of the ankle. By using the previous equations 3.8 the angular coefficient is \mathbf{m}_1 , and the known term is \mathbf{k}_1 . For the foot segment, (x_1, y_1) are the current coordinates of the heel, and (x_2, y_2) are the current coordinates of the mean position of the 1st and 5th toes. By

using the previous equations 3.8 the angular coefficient is \mathbf{m}_2 , and the known term is \mathbf{k}_2 . The angle formed by the two previous straight lines, the tibia and the foot, is defined by the equation 3.10. Also for the ankle angle it is possible considering two half-planes formed by the straight lines, and the sign of the angle is defined according to the position of the toes, or the belonging of the toes to one of the half-planes.

Using the method described in the previous paragraph, the hip, knee and ankle angles of the subject are extracted for all the walking sessions considering the Openpose output frame by frame. To obtain also the normalized angles of the subject, the static position has been considered as a reference and the three angles in the basic position are used as the zero of the subject.

$$\begin{cases} \alpha_{\text{Hip}}^{\text{Norm}} = \alpha_{\text{Hip}} - \delta_{\text{Hip}} \\ \alpha_{\text{Knee}}^{\text{Norm}} = \alpha_{\text{Knee}} - \delta_{\text{Knee}} \\ \alpha_{\text{Ankle}}^{\text{Norm}} = \alpha_{\text{Ankle}} - \delta_{\text{Ankle}}. \end{cases} \quad (3.11)$$

Table 3.8 shows the reference values in degrees of the three angles for each subject, obtained by using the coordinates of the Openpose key-points. In this case, the values refer to the lateral position of the subject. The reference values are defined as δ of the angles and are used in the 3.11 equations.

Table 3.8: Reference values of the angles obtained by the static position for each subject

	Subject 1	Subject 2	Subject 3	Subject 4	Subject 5
δ_{Hip} Right (degrees)	-8.3348	-2.2927	-1.2716	-8.1275	-9.9372
δ_{Knee} Right (degrees)	-2.4784	2.9073	3.0078	-4.2190	0.2208
δ_{Ankle} Right (degrees)	-7.6406	2.1897	1.8043	2.4322	-6.0922

3.2.6 Assessment of the length of the body segments

In the preliminary analysis carried out, some problems were identified in the functioning of the Openpose tool. Not being designed for its use in the clinic, an inaccuracy visually emerges to be faced for the most faithful construction of the subject's skeleton present in the images. Since the predictions of the landmark locations are made frame by frame, it is not taken into account the expectation of having a constant length of the body segments for the subject. Starting from the joint positions obtained as output from the Openpose system, the Euclidean distance between different points was calculated to observe the variation in the length of the main segments of the leg.

Considering the femoral segment, being (x_1, y_1) the current coordinates of the hip, and (x_2, y_2) the current coordinates of the knee, the length of the thigh is define as:

$$L_{Thigh} = \sqrt{(x_2 - x_1)^2 + (y_2 - y_1)^2}. \quad (3.12)$$

Considering the tibial segment, being (x_1, y_1) the current coordinates of the knee, and (x_2, y_2) the current coordinates of the ankle, the length of the shank is define as:

$$L_{Shank} = \sqrt{(x_2 - x_1)^2 + (y_2 - y_1)^2}. \quad (3.13)$$

Firstly, to correct this error, the length of the two body segments was calculated, in the static position, using the equations 3.12 and 3.13. Considering the confidence

Table 3.9: Values of the thigh and shank lengths for each subject considering the static position

	Subject 1	Subject 2	Subject 3	Subject 4	Subject 5
Thigh Length (pixel)	119.17	134.96	131.46	129.71	135.31
Shank Length (pixel)	100.43	114.26	116.01	114.69	124.84

values provided by the Openpose system, it is possible to ascertain, for all subjects and all sessions, that the most reliable joints are the knee and the ankle. In fact, for these landmarks, the prediction shows estimated averaged confidence values of around 0.8, moreover, the confidence of the ankle seems to be more constant than the other one, as shown in example in figure 3.19. For these reasons, it was decided to reconstruct the skeleton of the lower limb of the subject under examination starting from the ankle joint, and considering the segment length reported in table 3.8.

The steps for the reconstruction, frame by frame, of the lower limb are the following:

1. In the beginning, an anti-causal low-pass filter is applied to the hip trajectory to consider only the hip tilt. The cut-off frequency chosen is 10Hz, the order is 4, and the filter is Chebyshev type. The Openpose coordinates overtime of the hip, knee and ankle joints are stored in the variables: *HipCoord*, *KneeCoord*, and *AnkleCoord*. The lengths of the body segments, the shank, and the thigh, shown in the table 3.9 are considered. New variables are defined, in which the new joint coordinates will be saved: *HipNewCoord*, *KneeNewCoord*, and *AnkleNewCoord*. The first two are two-column variables, x , and y , in which only the coordinates of the joints of the first frame are known. All the rest of the variables are empty. On the other hand, all coordinates of the ankle joint are already stored in the new variable. So the variables *AnkleCoord*, and *AnkleNewCoord* are the same.

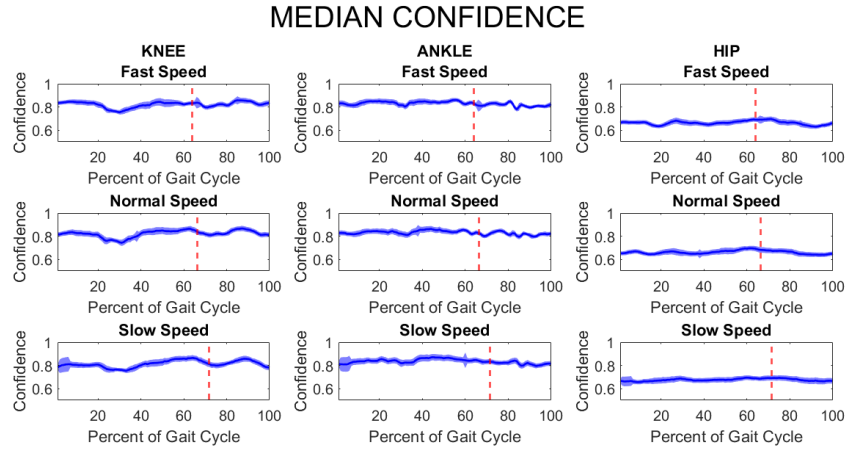


Figure 3.19: Median confidence of the Openpose system for one subject (subject 1)

2. The displacement of the ankle joint from the (i) -th position to the $(i + 1)$ -th position is considered, and it is called *AnkleMovement*. A new temporary knee position, called (i^{*+1}) -th, is defined by applying the same displacement *AnkleMovement*, or a rigid translation of the segment, to the (i) -th position of the knee.
3. The orientations of two straight lines are calculated: the first considers the segment formed by the position of the ankle $(i + 1)$ -th and the temporary position of the knee (i^{*+1}) -th; the second considers the position of the ankle $(i + 1)$ -th and the original position of the knee $(i + 1)$ -th. The rotation between the (i) -th frame and the $(i + 1)$ -th frame can be defined.
4. To obtain the final position of the knee at frame $(i + 1)$ -th, the previous rotation is applied to the shank segment at the frame (i) -th, also associating it with the correct length of the segment. The new obtained position of the knee is stored in the variable *KneeNewCoord* at position $(i + 1)$ -th.
5. Considering now the (i) -th and $(i + 1)$ -th knee new positions, the previous steps, from the second one, are repeated to obtain the new hip position which will be stored in the variable *HipNewCoord* at position $(i + 1)$ -th. The rotation of the thigh segment is applied, considering the correct length of the body segment.

The steps listed above are repeated for all the frames of the session, thus reconstructing the correct positions of the joints considering the constant length of the body segments. With each iteration, the previous position $(i + 1)$ -th becomes the new position (i) -th. In figure 3.20 is shown the process to define the new position of the knee joint in the $(i + 1)$ -th frame.

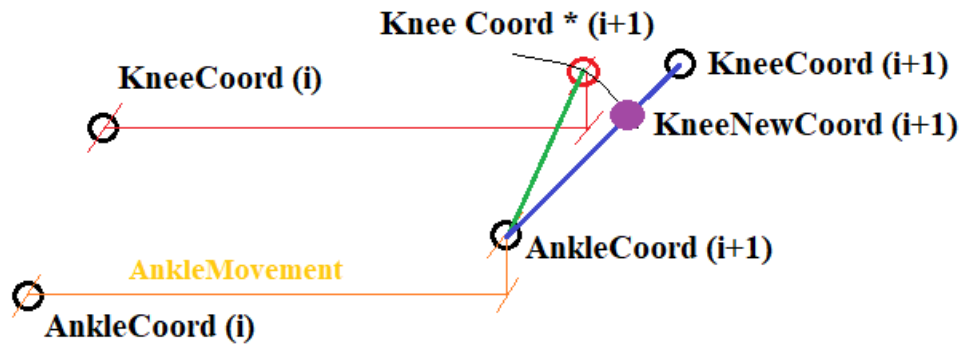


Figure 3.20: Representation of the method to reconstruct the leg by considering constant segment lengths

Chapter 4

Results and Discussion

In this chapter, both the results and the discussion are reported. In the first section, the results obtained in this preliminary analysis, the comparison of the gait data obtained by the Openpose tool and Vicon system, are shown. The second section discusses the previous results, defining the reliability of the tool in question and, eventually, the limits.

4.1 Results

The results presented in this section report the situations of the three different speeds used in the walking sessions: the fast, the normal and the slow speed. Each session lasts 2 minutes, and the first and second repetitions for each speed level are merged. The data has been sampled at 120 Hz . The data are divided into steps, using the RHS and RTO events, and each step has been resampled on one hundred points, by using a linear interpolation. The graphs showing the median and the standard deviation of the trend are obtained using the different steps available for each subject:

Table 4.1: Number of available steps for each subject

	Subject 1	Subject 2	Subject 3	Subject 4	Subject 5
Fast speed	272	241	279	236	246
Normal speed	220	205	226	198	203
Slow speed	149	146	157	144	139

4.1.1 Position of the centers of rotation

The first analysis that is carried out concerns the comparison of the positions of the body joints predicted by the Openpose tool with respect to the positions provided by the Vicon system. The interest is centered on the definition of the distances, reported in meter, between the Openpose estimated landmarks and the centers of rotation obtained by the Vicon markers positions, which is considered the gold standard.

The first parameter to calculate the distance of the corresponding joint positions of the two different systems is the mean absolute error [16], calculated for both the x-axis and y axes-axis:

$$MAE = \begin{cases} \frac{1}{n} \cdot \sum_{i=1}^n \|x_m(i) - x_o(i)\| \\ \frac{1}{n} \cdot \sum_{i=1}^n \|y_m(i) - y_o(i)\|, \end{cases} \quad (4.1)$$

where x_m is the current i -th position provided by the Vicon system, and x_o is the current i -th position estimated by the Openpose tool. The final MAE values, for each joint, is computed as the mean value obtained by the all n frames. In this case, the results of the different speed levels are merged.

Table 4.2: Distance, in meters, of the estimated Openpose landmarks and the Vicon centers of rotation

	Subject 1	Subject 2	Subject 3	Subject 4	Subject 5
Neck X (m)	0.051	0.042	0.049	0.052	0.045
Neck Y (m)	0.147	0.215	0.212	0.230	0.235
Hip X (m)	0.035	0.044	0.048	0.039	0.0359
Hip Y (m)	0.073	0.116	0.078	0.099	0.115
Knee X (m)	0.016	0.041	0.035	0.025	0.019
Knee Y (m)	0.053	0.075	0.059	0.063	0.045
Toe Med X (m)	0.019	0.017	0.015	0.032	0.029
Toe Med Y (m)	0.008	0.019	0.022	0.021	0.014
Toe Lat X (m)	0.012	0.031	0.023	0.023	0.015
Toe Lat Y (m)	0.007	0.025	0.019	0.018	0.011

The ankle joint is not reported in table 4.2 because the values are close to zero, so it is possible considering that the Openpose landmark and the Vicon center of rotation are in the same position.

The second parameter to calculate the distance between the joints is the Euclidean distance, obtained by the equation:

$$EuclideanDistance = \sqrt{(x_2 - x_1)^2 + (y_2 - y_1)^2}, \quad (4.2)$$

where (x_1, y_1) are the coordinates of the current frame of the current body joint obtained by the Vicon system, and (x_2, y_2) are the coordinates of the current frame of the current body joint predicted by the Openpose tool.

Table 4.3: Euclidean distance, in meters, of the estimated Openpose landmarks and the Vicon centers of rotation

	Subject 1	Subject 2	Subject 3	Subject 4	Subject 5
Neck (m)	0.049	0.044	0.046	0.054	0.053
Hip (m)	0.034	0.045	0.045	0.059	0.0049
Knee (m)	0.017	0.039	0.037	0.036	0.026
Toe Med (m)	0.018	0.018	0.020	0.043	0.030
Toe Lat (m)	0.012	0.035	0.024	0.034	0.017

The ankle joint is not reported in table 4.3 because the value of the euclidean distance is 0.003 meter for all the subjects.

4.1.2 Orientation of the body segments

The second analysis concerns the comparison of the orientation of the body segments. Starting from the positions of the markers given by the Vicon system, and the positions of the landmarks estimated by the Openpose instrument, the orientations of the three main segments of the lower limb are obtained: the thigh, the shank, and the foot.

Considering, for the femoral segment, (x_1, y_1) the coordinates of the hip and (x_2, y_2) the coordinates of the knee, the angle β , in degrees, between the segment axis and the horizontal axis is calculated as:

$$\begin{cases} m = \frac{y_2 - y_1}{x_2 - x_1} \\ \beta = \arctan(m). \end{cases} \quad (4.3)$$

In the same way the orientation of the tibial segment is calculated considering (x_1, y_1) the coordinates of the knee and (x_2, y_2) the coordinates of the ankle.

For the foot segment (x_1, y_1) are the coordinates of the heel and (x_2, y_2) are the coordinates of the toe (median position between the 1st and 5th toes).

For the same body segment, the orientations starting from the coordinates of the Vicon system (β_{VICON}) and the orientations starting from the coordinates of Openpose ($\beta_{OPENPOSE}$) are obtained. The difference in orientation is calculated for each body segment:

$$\delta\beta = \beta_{VICON} - \beta_{OPENPOSE}. \quad (4.4)$$

Obtained the differences $\delta\beta$ in the orientations of each of the three body segments, considering for each subject all the walking sessions, the average value, the standard deviation, the maximum and minimum values are obtained and reported in the tables 4.4, 4.5, and 4.6 .

Table 4.4: Mean value, standard deviation, maximum and minimum values of the differences in the thigh orientation for each subject

	Subject 1	Subject 2	Subject 3	Subject 4	Subject 5
Mean value	-0.2181	0.0472	-0.2040	-0.0022	-0.0969
Standard deviation	0.8784	0.8932	0.8235	0.6756	0.8315
Max value	3.1110	3.1177	3.1367	3.1359	3.1374
Min value	-3.1355	-3.1293	-3.1360	-3.1338	-3.1385

Table 4.5: Mean value, standard deviation, maximum and minimum values of the differences in the shank orientation for each subject

	Subject 1	Subject 2	Subject 3	Subject 4	Subject 5
Mean value	-0.0421	0.1179	-0.0654	0.0335	0.0369
Standard deviation	0.4299	0.6274	0.5223	0.4652	0.5964
Max value	3.1375	3.1384	3.1257	3.1201	3.1387
Min value	-3.1384	-3.1378	-3.1162	-3.1186	-3.1393

4.1.3 Angles of the lower limb

In this paragraph, the first evaluation concerns the method used to calculate the angles of the lower limb, which is described in the paragraph 3.2.5. The comparison concerns the angles provided by the Vicon system, and the angles obtained, using

Table 4.6: Mean value, standard deviation, maximum and minimum values of the differences in the foot orientation for each subject

	Subject 1	Subject 2	Subject 3	Subject 4	Subject 5
Mean value	-0.0844	0.0514	0.1148	0.0916	0.0064
Standard deviation	0.0971	0.3662	0.3627	0.5290	0.3424
Max value	2.1966	2.9327	2.7257	2.8037	3.1234
Min value	-0.7460	-2.1316	-1.8620	-2.4211	-3.1242

the method previously mentioned, starting from the coordinates of the centers of rotation provided by the Vicon system. In this way, it is possible to observe whether the calculations performed to obtain the hip, knee, and ankle angles are correct. Figures 4.1 and 4.2 show the angles of the three main joints of the lower limb to be compared.

Initially, the comparison is carried out by comparing, in both previous cases, the angles of the same step isolated thanks to the events of RHS and RTO. The distance between the step provided by the Vicon system, shown in figure 4.1, and the step obtained with the method described in this thesis work, shown in figure 4.2, is then calculated as the difference, step by step, between the two methods. Obtained all the distances between the two types of angle correspondingly for each step, the median and the standard deviation of the previously obtained differences are calculated.

As can be seen in the figures 4.3, there is a considerable distance in calculating the hip angle. This error, of the method used, is almost constant during the gait cycle and it is around twenty degrees for all subjects analyzed. There is an underestimate in the calculation of the hip angle using the method described in paragraph 3.2.5, as can be seen in figure 4.4. In table 4.7, the mean distances for the hip angle is reported for all the subjects.

Table 4.7: The average distances between the hip angles provided by the Vicon system and the hip angles calculated with the method used for this thesis work

	Subject 1	Subject 2	Subject 3	Subject 4	Subject 5
Mean distance (degrees)	21.72	20.53	21.42	18.18	17.29

This error is corrected in the calculation of the hip angles, obtaining the following results reported as the median angle and standard deviation (figure 4.5).

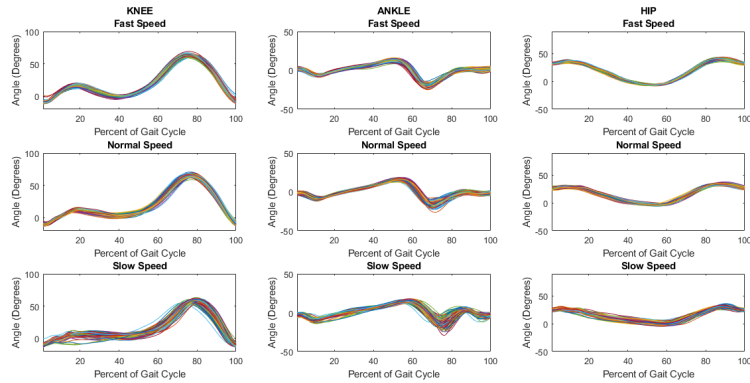


Figure 4.1: Hip, knee, and ankle angles provided by the Vicon system (subject 1)

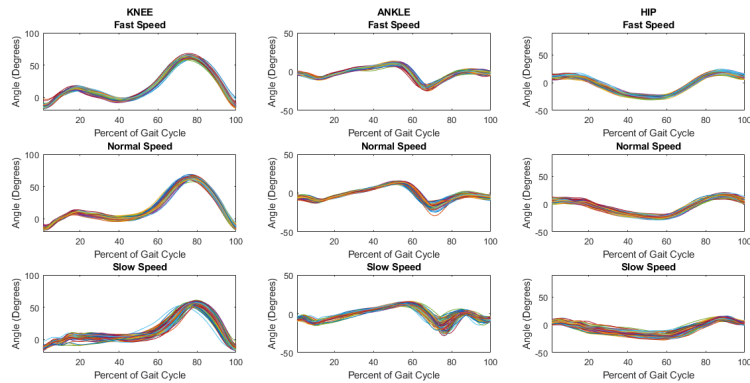


Figure 4.2: Hip, knee, and ankle angles obtained from the positions of the centers of rotation provided by the Vicon system (subject 1)

After compensating the bias previously observed in calculating the hip angles, the distances between the angles is recalculated, resulting in errors of less than five degrees for the three main angles of the lower limb for all the subjects (figure 4.6). Table 4.8 reports the maximum values of the errors obtained for each subject. A statistical value in the estimation of the angles is reported by calculating the root mean square error. The RMSE indicates the discrepancy between the values of the observed data, the Vicon angles in this case, and the values of the estimated data, the angles calculated starting from the positions of the centers of rotation.

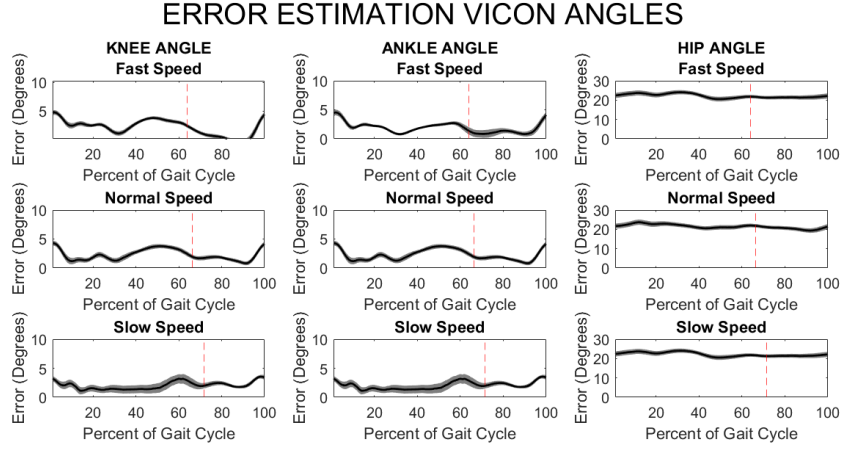


Figure 4.3: Median distance and standard deviation between the angles provided by the Vicon system and the angles obtained with the method described in paragraph 3.2.5 (subject 1)

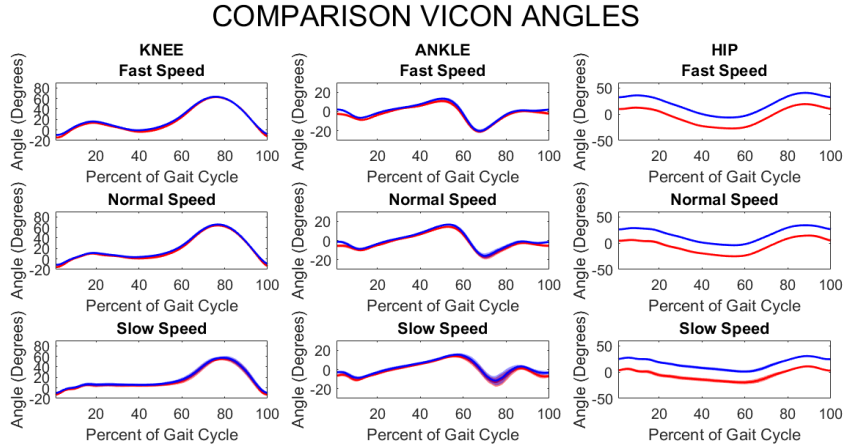


Figure 4.4: Hip, knee, and ankle angles provided by the Vicon system, in blue, and angles obtained with the method described in this thesis, in red.

$$RMSE = \sqrt{\sum_{i=1}^n \frac{(\gamma_1 - \gamma_2)^2}{n}}, \quad (4.5)$$

where γ_1 is the current Vicon angle of the current step, and γ_2 is the current angle calculated of the current step. For each step, a value of RMSE is obtained, by considering all the angles of the entire gait cycle.

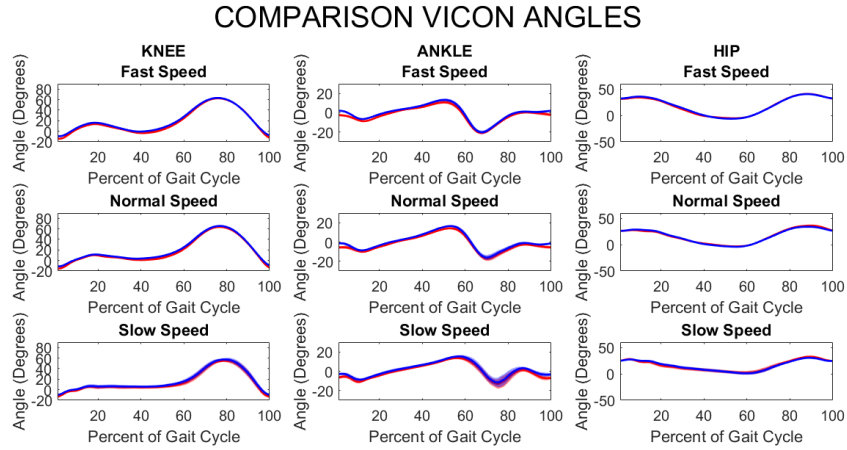


Figure 4.5: Hip, knee, and ankle angles provided by the Vicon system, in blue, and corrected angles obtained with the method described in this thesis, in red.

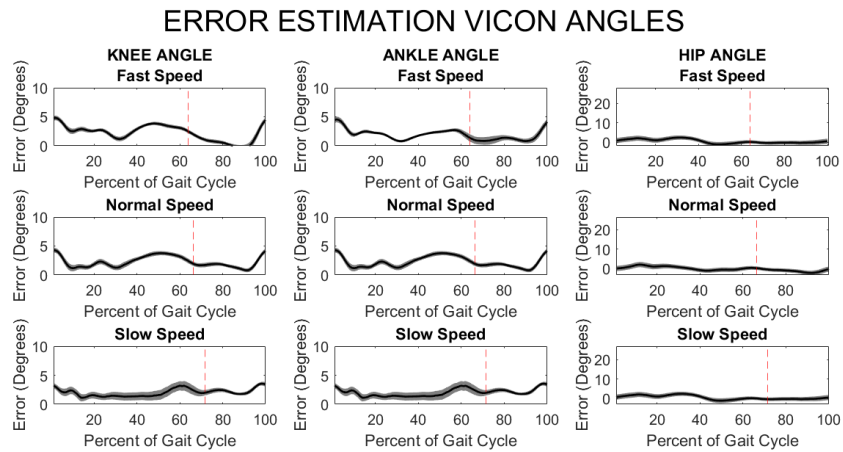


Figure 4.6: Median distance and standard deviation between the angles provided by the Vicon system and the angles obtained with the method described in paragraph 3.2.5, after compensating the bias in the hip angles

Table 4.9 shows the average values of the RMSE for each subject.

The second evaluation regards the comparison of the hip, knee and ankle angles provided by the Vicon system and the same angles obtained starting from the predicted positions of the landmarks by the Openpose instrument. Figure 4.8 shows the angles of the hip, knee, and ankle obtained using the method described in paragraph 3.2.5 starting from the coordinates of Openpose. The angles of all

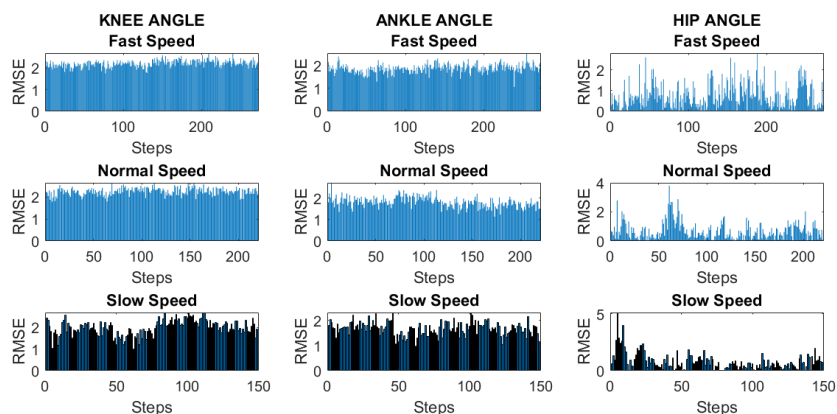


Figure 4.7: RMSE calculated for each step, between the Vicon angles and the correspondent angles calculated by using the method in the paragraph 3.2.5 (subject 1)

Table 4.8: Maximum values of the distance between the Vicon angles and the correspondent angles calculated by using the method in the paragraph 3.2.5 for each subject

	Subject 1	Subject 2	Subject 3	Subject 4	Subject 5
Hip Angles (degrees)	2.49	3.64	4.11	2.28	5.03
Knee Angles (degrees)	4.81	2.87	3.77	2.71	1.66
Ankle Angles (degrees)	4.54	3.86	4.83	3.32	2.51

the steps are shown superimposed, isolated using the events of RHS and RTO. In the same way, as in the previous evaluation, the distances and the root mean square errors are calculated, for each step, between the angles of a gait cycle provided by the Vicon system and the angles obtained from the Openpose coordinates. Tables 4.10 and 4.11 show the results obtained for the five subjects; in particular, the first table shows the mean values of the distances obtained in the gait cycle between the hip, knee and ankle angles provided by the Vicon system and the same angles obtained by the landmarks predicted by Openpose; the second table instead shows the average value of the root mean square error calculated considering the two methods. The figures below (4.9, 4.11, 4.13, 4.10, 4.12, 4.14) show the results obtained for three significant subjects analyzed, with the different presence of noise in the data.

Table 4.9: Average RMSE values obtained from the Vicon angles and the correspondent angles calculated by using the method in the paragraph 3.2.5 for each subject

	Subject 1	Subject 2	Subject 3	Subject 4	Subject 5
Hip Angles (degrees)	0.62	0.86	2.09	0.83	0.66
Knee Angles (degrees)	2.26	0.73	0.39	0.28	0.69
Ankle Angles (degrees)	1.79	1.84	1.96	1.32	1.13

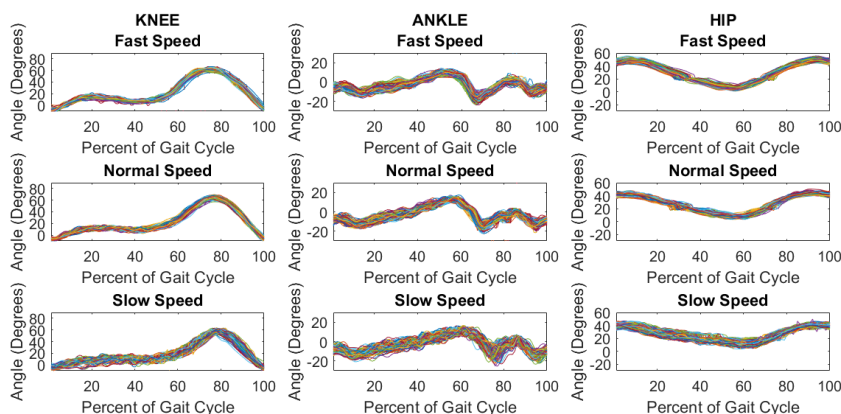


Figure 4.8: Hip, knee, and ankle angles obtained starting from the positions of the predicted landmarks provided by the Openpose tool (subject 1)

4.2 Discussion

This section discusses the previously reported results. The results obtained in terms of the positions of the centers of rotation, the orientations of the body segments and the lower limb angles, are discussed separately.

4.2.1 Position of the centers of rotation

The data concerning the landmarks' positions predicted by the Openpose tool are compared with the centers of rotations provided by the Vicon system through two different parameters.

The first parameter is the MAE, calculated for all the main anatomical points along both the x-axis and y-axis. As can be seen from the values shown in the table 4.2, the greatest discrepancies in the position of the landmarks are encountered for the neck and the hip. Considering the joint of the neck, this difference along

Table 4.10: Average values of the distance between the Vicon angles and the Openpose angles calculated by using the method in the paragraph 3.2.5 for each subject

	Subject 1	Subject 2	Subject 3	Subject 4	Subject 5
Hip Angles (degrees)	10.79	5.23	4.47	8.48	7.03
Knee Angles (degrees)	3.27	3.51	3.31	2.34	3.64
Ankle Angles (degrees)	5.08	3.82	3.65	5.31	4.02

Table 4.11: Average RMSE values obtained from the Vicon angles and the Openpose angles calculated by using the method in the paragraph 3.2.5 for each subject

	Subject 1	Subject 2	Subject 3	Subject 4	Subject 5
Hip Angles (degrees)	10,81	2.32	2.14	7.11	7.01
Knee Angles (degrees)	2.27	1.82	1.32	3.76	5.91
Ankle Angles (degrees)	4.48	3.93	4.15	7.36	4.25

the axes is not seen as a malfunction of the instrument under analysis but it is given by the different definitions of the neck joint in the two systems. The Vicon system assigns to this landmark the coordinates of the marker positioned on the C7 vertebra, while Openpose positions this joint close to the center of the clavicle, in the middle position between the two shoulders. It can be therefore considered the reported distances as the anatomic distances between the two points considered by the different systems.

As for the points positioned on the foot, there are small distances, in the worst case, of about 3 centimeters. It can be considered that the ankle is in the same position for the two systems, and some uncertainties instead result in the other points of the foot.

From the results reported, the difficulty of the tool in the analysis of positioning the joint of the hip is evident, probably due to the lack of details in the area, that can not focus the recognition of the point.

The identification of the knee height, therefore along the y-axis, in some subjects is not precise.

The second parameter instead gives a more general idea of the distances of the points, underlining the greater direction of distance, but highlighting the centimeters of real distances between them. As can be seen in table 4.3, the Euclidean distances

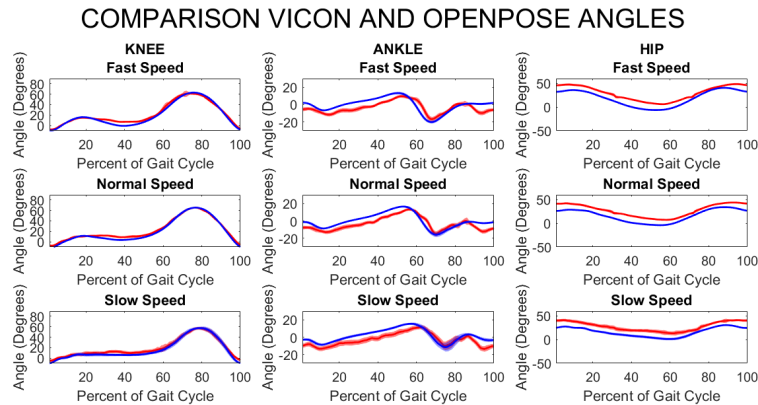


Figure 4.9: Hip, knee and ankle angles provided by the Vicon system, in blue, and Openpose angles obtained with the method described in paragraph 3.2.5, in red (subject 1)

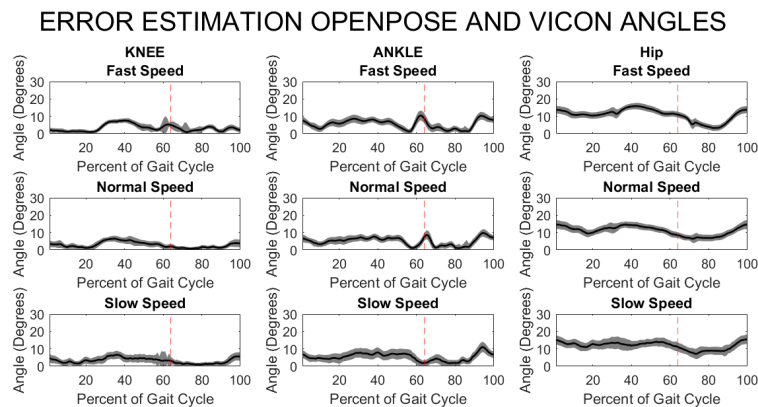


Figure 4.10: Median distance and standard deviation between the angles provided by the Vicon system and the Openpose angles obtained with the method described in paragraph 3.2.5 (subject 1)

obtained once again highlight the previous discrepancies for the neck and hip points, with average distances of about 5 cm for the neck and 4 cm for the hip. For the knee joint, there is also an inaccuracy of about 2.5 cm on average in predicting the real position of the center of rotation, while it is evident a lower difficulty in the definition of the points of the foot.

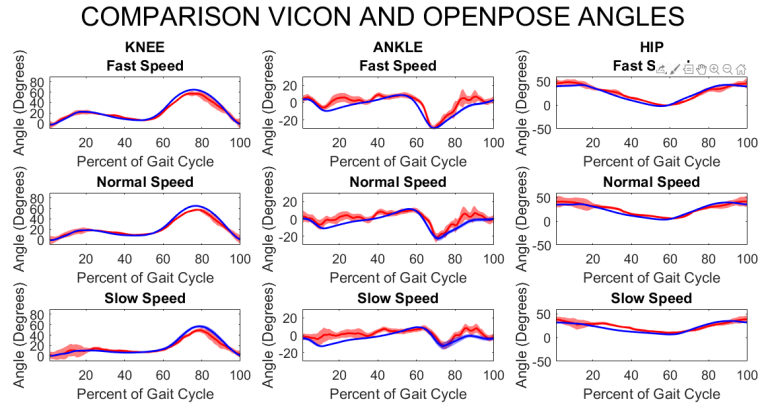


Figure 4.11: Hip, knee and ankle angles provided by the Vicon system, in blue, and Openpose angles obtained with the method described in paragraph 3.2.5, in red (subject 2)

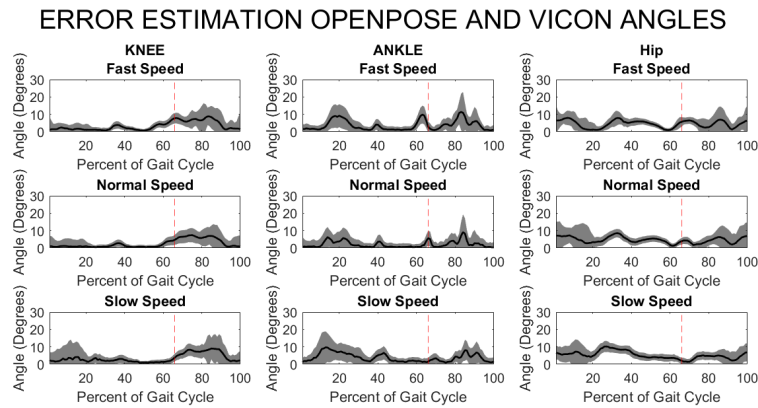


Figure 4.12: Median distance and standard deviation between the angles provided by the Vicon system and the Openpose angles obtained with the method described in paragraph 3.2.5 (subject 2)

4.2.2 Orientation of the body segments

Considering the results obtained in the analysis of the orientations of the three body segments, it is noted that, on average, there are no large discrepancies between the orientations of the Vicon segments compared to those obtained with the Openpose data. In fact, from the data reported in table 4.4 and 4.5, it can be observed that the differences in orientations, of the thigh and shank, are more or less 3 degrees approximately. The maximum differences between the two systems in the

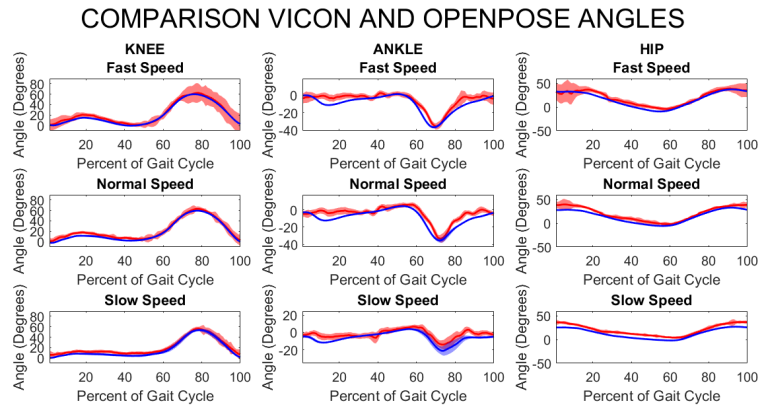


Figure 4.13: Hip, knee and ankle angles provided by the Vicon system, in blue, and Openpose angles obtained with the method described in paragraph 3.2.5, in red (subject 5)

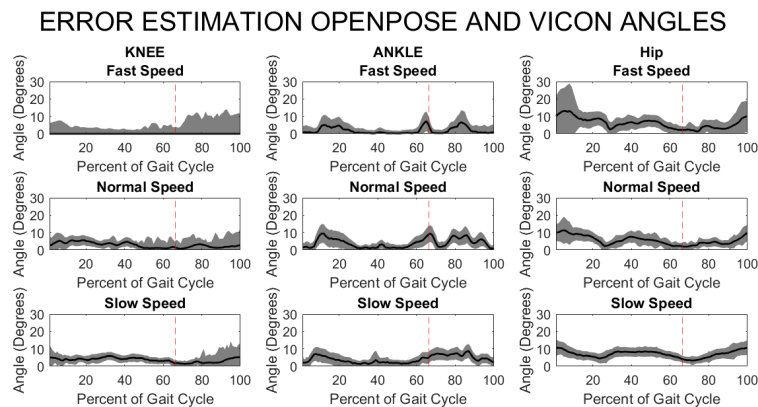


Figure 4.14: Median distance and standard deviation between the angles provided by the Vicon system and the Openpose angles obtained with the method described in paragraph 3.2.5 (subject 5)

orientation of the foot segment is about one degree lower than the previous ones, as can be seen in table 4.6.

Therefore, there are no evident problems in the estimation, by the Openpose tool, of the orientations of the main three body segments of the lower limb.

4.2.3 Angles of the lower limb

The first results to be discussed in this section concern the angles provided by the Vicon system and the angles calculated from the Vicon positions of the centers of rotation. Visually a bias is observed in figure 4.3 that shows the average difference between the angles under examination. After calculating the median bias for each subject, it can be observed that the method of paragraph 3.2.5 makes an error of about twenty degrees in the calculation of the hip angle. This error could be the result of different definitions of the hip angle: the consideration of different segments for the computing of the values. Anatomically the hip angle is defined as the angle between the axis of the pelvis and the axis of the femur, that is the definition followed by the Vicon system. Considering the lateral pictures, provided to the Openpose tool, it is impossible the observation of the right pelvis segment. For this reason, the hip angle is computed by considering another segment instead of the pelvis one: the new segment is defined as the perpendicular segment concerning the trunk segment. This measure could, therefore, result in an underestimation of the hip angle, represented as an almost constant bias of similar value for all the subjects analyzed, as can be seen in figure 4.4. As can be seen in the table 4.8, after correcting the bias discussed above, the maximum error obtained in calculating the three angles in question does not exceed 5 degrees. The calculated RMSE values are also acceptable, with a maximum of 2 degrees for the worst cases reported in table 4.9.

The second results to be discussed in this section concern the angles provided by the Vicon system and the angles calculated from the Openpose positions of the predicted landmarks. By observing the values shown in the table 4.10, it can be defined that, on average, the error in calculating the hip angle is 10 degrees, probably due to the uncertainty still present in the instrument that predicts the position of the hip. Furthermore, in the figures showing three cases of average distances between the angles obtained in the two methods (4.10, 4.12, 4.14), an average maximum error is observed in the calculation of the angle of about 13 degrees. For the noisiest subjects, a high standard deviation is observed in the figures listed above. As regards the other two angles of the lower limb, the average error in calculating the values is much less. Table 4.10 shows an average maximum error of about 5 degrees for both the knee angle and the ankle angle. The same observations can be made by observing the RMSE values reported in table 4.11. A high error value can be observed for the hip angle.

Chapter 5

Possible Medical Application and Future Goals

5.1 Medical application

This section presents the introduction to a possible medical application of the Openpose tool in question. The idea was born in Boston at the Spaulding Rehabilitation Hospital, where patients with different pathologies are followed for rehabilitation. Following the evaluations made on the practicality and on the necessary times of the traditional Vicon system for gait analysis, it was decided to think of an alternative method for such analyzes. In particular, clinicians found difficulties in studying children's gait. The system used is cumbersome, and a long preparation is required to collect the data. Besides, clinicians suggest finding a method to ensure patient follow-up during the rehabilitation process, at the moment not possible as the laboratory set-up specifically for gait analysis is required.

The medical application suggested concerns the analysis of the gait of children with cerebral palsy by using the Openpose tool. If such an application is made possible, patients could be followed during rehabilitation, with the only use of standard cameras.

5.1.1 Cerebral palsy disease

Infantile CP is one of the most common childhood diseases, there are 500,000 affected children in the USA alone, and it is a persistent, and not progressive disease of the posture and the movements, due to changes in the brain function before the central nervous system has completed its development, or due to damage

that occurs during the prenatal, perinatal or postnatal periods. Often, symptoms include poor coordination, stiff and weak muscles, and tremors. It can be noted, in children with this pathology, difficulty in the movements that affect the limbs above all. For this reason, the gait of the CP children is uncoordinated and difficult. With constant rehabilitation sessions, which is a lifelong therapy, it is possible to improve the quality of walking of the patients. The problem encountered in the follow-up sessions, for the evaluation of rehabilitation and interventions, is the difficulty in planning constant visits. To date, children are followed by clinicians who visually attribute scores based on the type of walk, or a traditional motion analysis system is used to have more precise values. Since data collection and data analysis require a long time (at least 2 hours), the visits are carried out only in particular circumstances. As can be seen in figure 5.1, many markers are needed, attached to the subject's body, in certain anatomical points.



Figure 5.1: Example of a session of a child with CP in the Motion Analysis Lab at the Spaulding Rehabilitation Hospital

To make patient follow-up more accessible, faster and at a lower cost, it would be useful the use of a pose estimation tool to obtain gait data. In this regard, tests of the use of Openpose were carried out on some subjects affected by CP at the Spaulding Rehabilitation Hospital's laboratory. In figures 5.2 and 5.3 examples of Openpose output are presented.

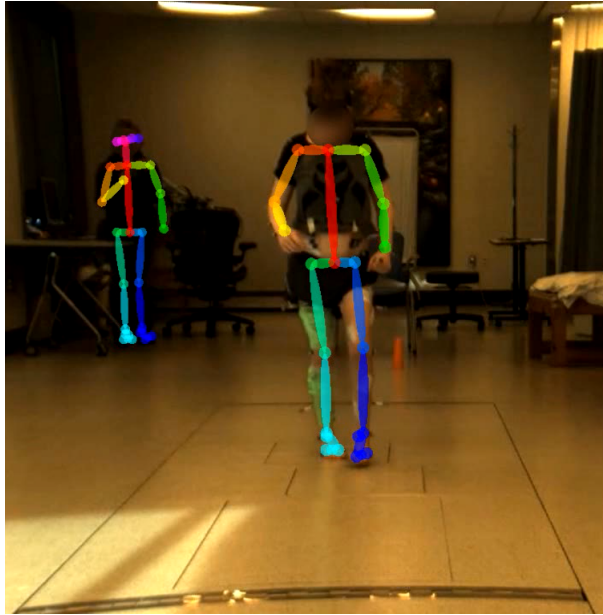


Figure 5.2: Example of the Openpose output of a child with CP in the Motion Analysis Lab at the Spaulding Rehabilitation Hospital

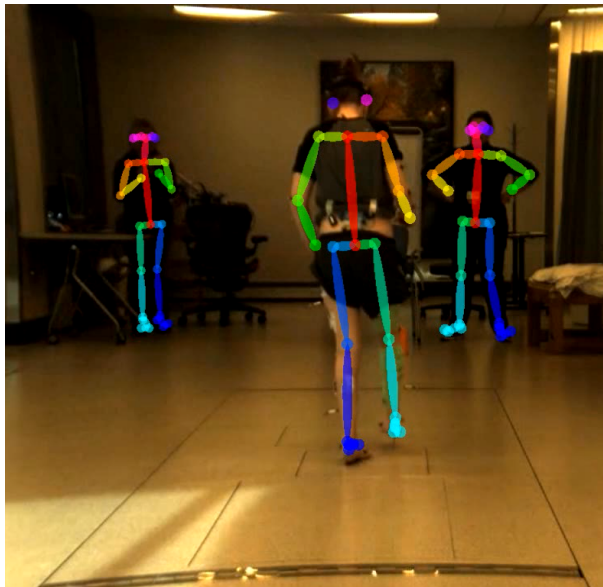


Figure 5.3: Example of the Openpose output of a child with CP in the Motion Analysis Lab at the Spaulding Rehabilitation Hospital

The analysis of data in a subject that is moving concerning the cameras is more complicated than the preliminary analysis presented in the previous chapters. Furthermore, Openpose's prediction regarding the location of landmarks is not accurate enough and quantitative analysis of gait abnormalities is not possible. For this reason, it was decided to start carrying out a more qualitative analysis of the gait, for example following the improvement of patients undergoing rehabilitation with the attribution of scores. Considering CP patients, the Edinburgh scale can be a guideline in this regard [17]. Since this scale presents a classification of the patient's severity considering the range of angles and not precise angles, Openpose accuracy may be sufficient for simple follow-up.

5.2 Future goals

This chapter presents possible future developments that could solve the problems and limitations shown in this thesis work. In fact, Openpose is still not sufficiently accurate to be used for the evaluation of gait abnormalities, not having been designed for medical applications. Considering the long-term objective of the project, the idea is to replace the traditional Vicon system with a user-friendly and low-cost system to perform longitudinal evaluations of gait quality on patients, ensuring an adequate and efficient follow-up.

The first option could be the use, in addition to the pose estimation tool, of new hardware components that can provide complementary information to Openpose. The idea is the use of some radio tags, that provide ultra-wide bandwidth signals, to determine biomechanical constraints in addition to the previous machine learning algorithm output. The use of the Openpose tool is useful to obtain gross estimates of the gait kinematics, while the use of radio tags positioned on certain anatomical landmarks is useful to refine the previous estimates. Following the preliminary analysis carried out in this thesis work, a possible positioning of the component on the pelvis is suggested, because of the not accurate prediction of this anatomical point. In this way, by adjusting the position of the hip, the results obtained for the analysis of the gait can be improved.

Besides, it might be useful to deeply study the code of the machine learning algorithm, improving and strengthening the tracking of landmarks frame by frame. It would be useful to look for the same landmark in the next frame considering some limits, therefore a maximum area in which it is expected the new position or the maximum displacement allowed. In this way, sudden and abrupt movements of the landmarks would be avoided, obtaining smoother signals.

The other improvement could be the merging of the frontal and lateral views of the cameras then obtaining more precisely the position of the landmarks in the space. The open-source Openpose tool [18] is continually updated, and the 3D tracking

TABLE 1. *Edinburgh visual gait score chart*

Foot	Stance				
	Flexion 2	1	Normal 0	1	Extension 2
1. Initial contact			Heel contact	Flatfoot contact	Toe contact
2. Heel lift	No forefoot contact	Delayed	Normal	Early	No heel contact
3. Max ankle dorsiflexion	Excessive dorsiflxn (>40° df)	Increased dorsiflxn (26°–40° df)	Normal dorsiflxn (5°–25° df)	Reduced dorsiflxn (10° pl–4° df)	Marked plantarflxn (>10° pl)
4. Hindfoot varus/valgus	Severe valgus	Mod valgus	Neutral/slight valgus	Mild varus	Severe varus
5. Foot rotation	Marked extn >KPA (by >40°)	Mod ext >KPA (by 21°–40°)	SI more extn than KPA (by 0°–20°)	Mod int >KPA (by 1°–25°)	Marked int >KPA (by >25°)
Knee					
8. Knee progression angle	External, part knee cap visible	External, all knee cap visible	Neutral, knee cap midline	Internal, all knee cap visible	Internal, part knee cap visible
9. Peak extn stance	Severe flxn (>25°)	Mod flxn (16°–25°)	Normal (0°–15° flxn)	Mod hyperextn (1°–10°)	Severe hyperextn (>10°)
Hip					
12. Peak extn stance	Severe flxn (>15°)	Mod flxn (1°–15° flxn)	Normal (0°–20° extn)	Mod hyperextn (21°–35° extn)	Marked hyperextn (>35°)
Pelvis					
14. Obliquity at mid stance	Marked down (>10°)	Mod down (1°–10°)	Normal obliquity (0°–5° up)	Mod up (6°–15°)	Marked up (>15°)
15. Rotation at mid stance	Marked retraction (>15°)	Mod retraction (6°–15°)	Normal (5° retr–10° pro)	Mod protraction (11°–20°)	Severe protraction (>20°)
Trunk					
16. Peak sagittal position	Marked forward	Mod forward lean	Normal upright	Mod backward lean	N/A
17. Max lateral shift	Marked	Mod	Normal	Reduced	N/A

(Table continued)

Figure 5.4: Guidelines table for classifying CP patients according to the Edinburgh scale [17], considering the lower limb angles during the stance phase of the GC

TABLE 1. (Continued)

Foot	Swing				
	Flexion 2	1	Normal 0	1	Extension 2
6. Clearance in swing		High steps	Full	Reduced	None
7. Max ankle dorsiflexion	Excessive dorsiflxn (>30° df)	Increased dorsiflxn (16°–30° df)	Normal dorsiflxn (15° df–5° pl)	Mod plantarflxn (6°–20° pl)	Marked plantarflxn (>20° pl)
Knee					
10. Terminal swing	Severe flxn (>30°)	Mod flxn (16°–30°)	Normal (5°–15° flxn)	Mod overextn (4° flx–10° xtn)	Severe hyperextn (>10° xtn)
11. Peak flxn swing	Severely increased (>85° flxn)	Mod increased (71°–85° flxn)	Normal (50°–70° flxn)	Mod reduced (35°–49° flxn)	Severely reduced (<35° flxn)
Hip					
13. Peak flexion swing	Marked increase (>60° flxn)	Increased flxn (46°–60° flxn)	Normal flxn (25°–45° flxn)	Reduced flxn (10°–24° flxn)	Severely reduced (<10° flxn)

Figure 5.5: Guidelines table for classifying CP patients according to the Edinburgh scale [17], considering the lower limb angles during the swing phase of the GC

of landmarks has been published with the possibility of the reconstruction of the subject’s skeleton in space (figure 5.6).

Furthermore, it would be useful, at a clinical level, to study the angles of the lower limb, the rotations of the body segments and the position of the landmarks also from other points of view, which have not been studied in-depth in this work.

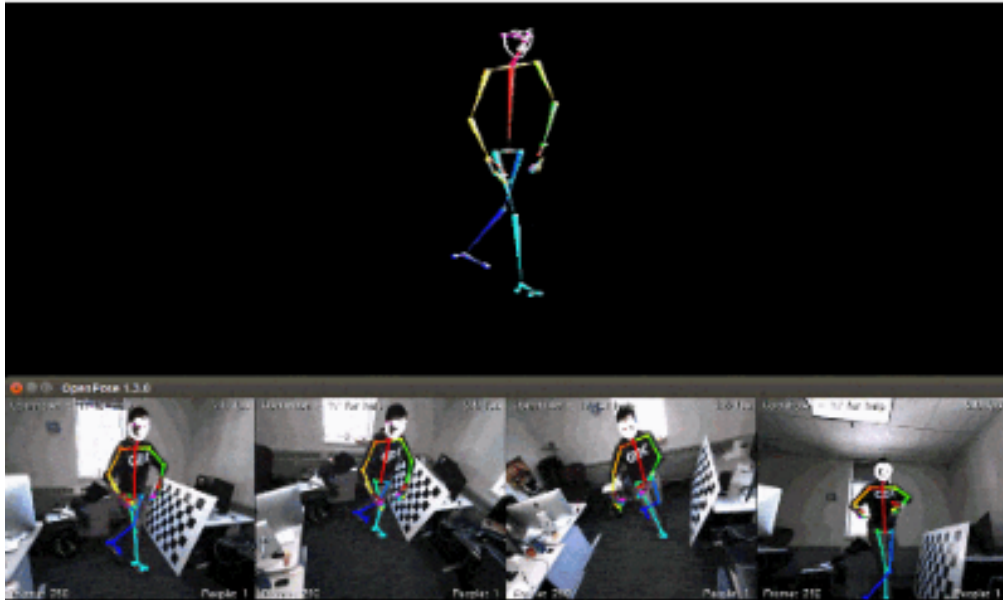


Figure 5.6: Example of the 3D reconstruction, by the Openpose tool, of the body skeleton starting from different cameras and different points of view [18]

Chapter 6

Conclusion

This thesis work presents a preliminary assessment of a pose estimation tool, called Openpose, intending to evaluate its possible use in the medical field, in particular, its use in the motion analysis laboratories. Since traditional gait analysis systems require lengthy preparation of the subject, they are expensive and can only be used in specific laboratories, there is a need to develop new systems that are more easily usable.

To date, research is moving towards the development of systems that can provide information on the gait with the use of only standard video-cameras and without the use of markers. Different machine learning algorithms can be used to extrapolate the gait data from the images captured during the data collection. In this work, among the new attractive machine learning algorithms introduced in the field of data science, the behavior of Openpose has been analyzed.

The evaluation was carried out comparing the data provided by the traditional Vicon system, generally used for gait analysis in the motion laboratories, and the data obtained by Openpose, the new open-source tool under examination. For the analysis, the attention was focused, for both systems, on the position of the centers of rotation, the orientation of the body segments, and the angles of the lower limb (the hip, the knee, and the ankle angles). The data provided by the traditional gait analysis Vicon system are considered as the gold standard for the comparison. The experiment was conducted with 5 healthy subjects, with no posture or motor impairments, who performed several treadmill walking sessions. The videos recorded, by two standard cameras, were provided to the Openpose tool, which predicted the coordinates of the body landmarks frame by frame. The passive markers were traced from the Vicon system cameras and the positions of the centers of rotation were obtained.

The analysis carried out highlights problems in the Openpose positioning of the joint of the hip starting from the videos, with average discrepancies of 4 cm concerning the Vicon positions. On the other hand, the estimate of the rotation of the body

segments is sufficiently accurate, with an inaccuracy of a maximum of 3 degrees for all the lower limb segments.

As regards the extraction of the lower limb angles, it can be said that the algorithm used for the calculation of the hip, knee and ankle angles is validated and it allows obtaining values with maximum errors of 5 degrees, in the worst cases.

Comparing the final angles obtained by the Openpose tool and the Vicon system, an average error of 5 degrees is observed for all the three angles, with maximum peaks around 10 degrees in the worst conditions.

In conclusion, the Openpose tool for the moment is not sufficiently accurate to quantitatively evaluate the gait abnormalities of subjects suffering from serious diseases and disabilities. Although the limitations observed, it can be considered promising for constant qualitative analyzes, and it can be taken into account as a starting point for a future more accurate marker-less system for gait analysis.

Appendix A

Guide to using Openpose

A brief guide on the use of the Openpose tool is provided in this appendix. First of all, the tool in question can be used on various platforms, such as Ubuntu, Windows, Mac OSX, and embedded systems.

Furthermore, different types of hardware can be used, CUDA GPUs, OpenCL GPUs, and CPU-only devices, with different qualities in terms of computational time above all and keeping the high quality [13].

At this link <https://github.com/CMU-Perceptual-Computing-Lab/openpose> [18] it is possible to find the real-time multi-person keypoint detection library, a Quick Start guide of the tool, and all the information related to the use of Openpose. After installing the library, you can use the tool by writing commands on any command-line interface program, such as Terminal, Terminator, PowerShell or Windows CMD Command Prompt.

You can choose the model to be applied to the reconstruction of the human skeleton, depending on the anatomical points of interest. The possible models are COCO (figure A.2) and MPI, that are slower and less accurate, or BODY 25 (figure A.1), suggested as faster and it includes both body and foot key-points.

The input of the system can be a video, some images or a webcam.

Below some code examples are reported.

```
./build/examples/openpose/openpose.bin --image_dir examples/media/  
  
--write_images output_folder_path/ --write_images_format jpg  
  
--write_json output_folder_path/
```

The format of the Openpose output is JSON file type, which can be easily decoded in Matlab via the *jsondecode* function.

```
filename=jsondecode(fileread('filename.json'));
```

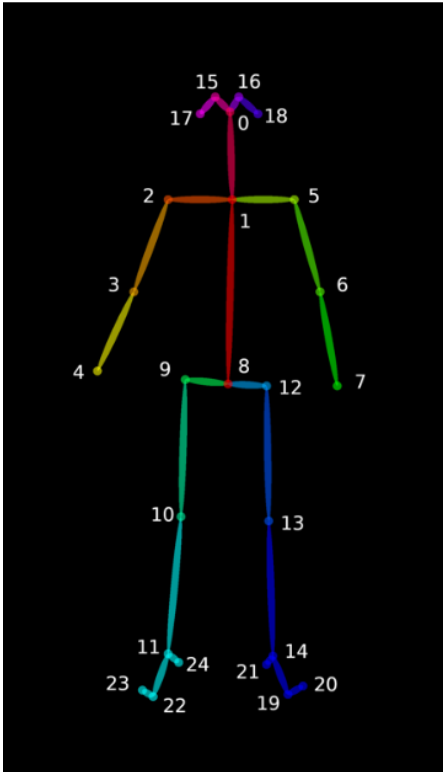


Figure A.1: BODY-25 model [13]

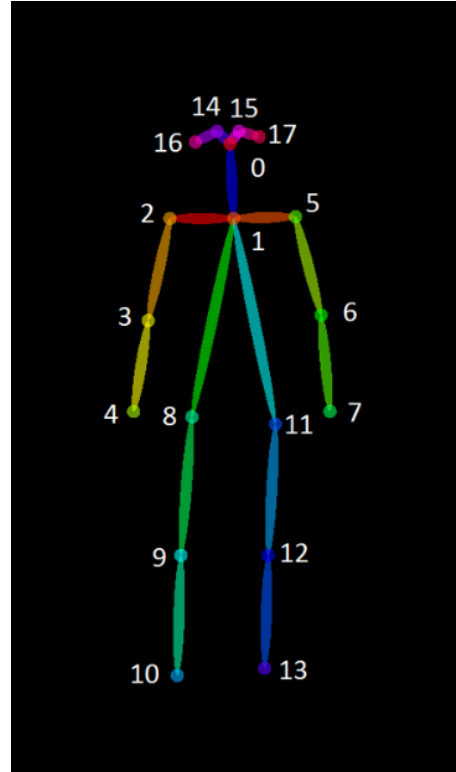


Figure A.2: COCO model [13]

In this thesis work the BODY-25 model was used. The output of Openpose is a structure in which the coordinates of the twenty-five key points are stored. In particular, for each point of the skeleton, the x-coordinate, the y-coordinate, and the confidence (it indicates how sure is the algorithm that the body's part is located in that pixel position) are given.

Appendix B

Guide to using the Camera Calibration Matlab tool

In this thesis work the 'Matlab R2019b' version is used [14]. The steps, necessary for the calibration of a single camera, are listed below. A recorded video in which a chessboard appears in different positions is necessary.

1. First of all, it is necessary to open the calibrator tool [15] by typing *cameraCalibrator* on the command line or to select it from the desktop Apps tab. Once the application screen is open, it is necessary to select the images previously placed in a folder, in which the chessboard appears in different positions (figure B.1).
2. After selecting the images showing the chessboard in different positions concerning the camera, the size of the squares on the chessboard, used as the calibration tool, is requested. In this case 23 mm (figure B.2). The tool detects then the chessboard in each provided image; if the chessboard is not clearly shown in some pictures, not all the loaded images may be used by the calibrator, as it is not able to recognize the chessboard in them (figure B.3). The app then shows the images with the chessboard detected, so it is possible to visually check that the tool has not made any mistakes in the search (figure B.4).
3. Subsequently, it is possible to calibrate the instrument to calculate the parameters of the camera lenses, starting from the data relating to the chessboard previously taken (figure B.5). The tool returns the first data results visually through three windows, that show the bar histogram of the reprojection errors (figure B.6), and both the camera-centric and the pattern-centric for each picture (figure B.7).

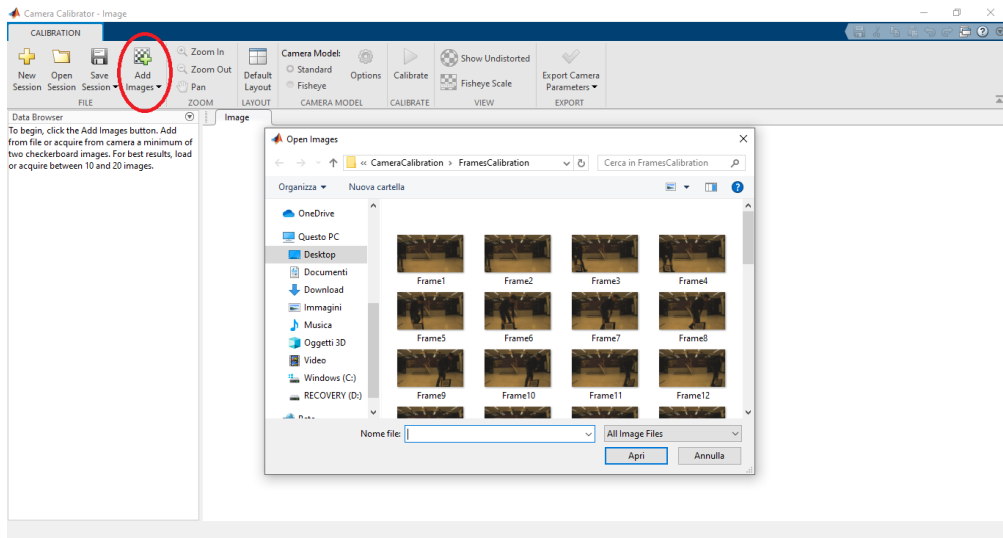


Figure B.1: The first screen of the application: the images, in which the chessboard is visible, are uploaded

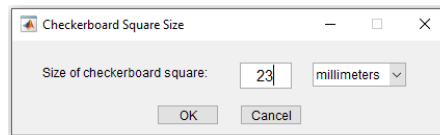


Figure B.2: The second screen of the application: window for the definition of the size of the chessboard squares

4. To verify the success of the estimation of the camera parameters, it is possible to view the previously loaded images without distortion. Finally, the tool allows you to extract the final parameters and to save them in a Matlab structure (figure B.9).

The Matlab tool returns all the calculated parameters and the matrices necessary to be able to eliminate distortions from the images. By using the ***undistortImage*** function it is possible to return all the undistorted frames of a video recording, recorded using the camera previously calibrated.

The figure B.10 shows the chessboard used for this thesis work.

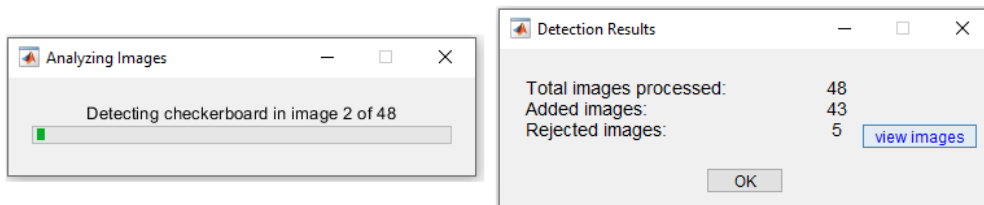


Figure B.3: The third screen of the application: window showing the chessboard detection result

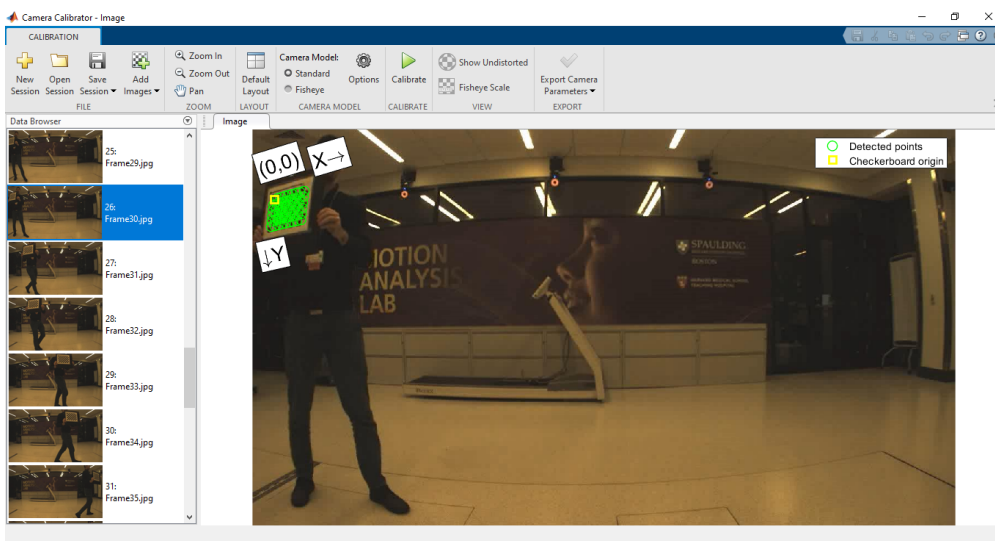


Figure B.4: Result of the chessboard detection

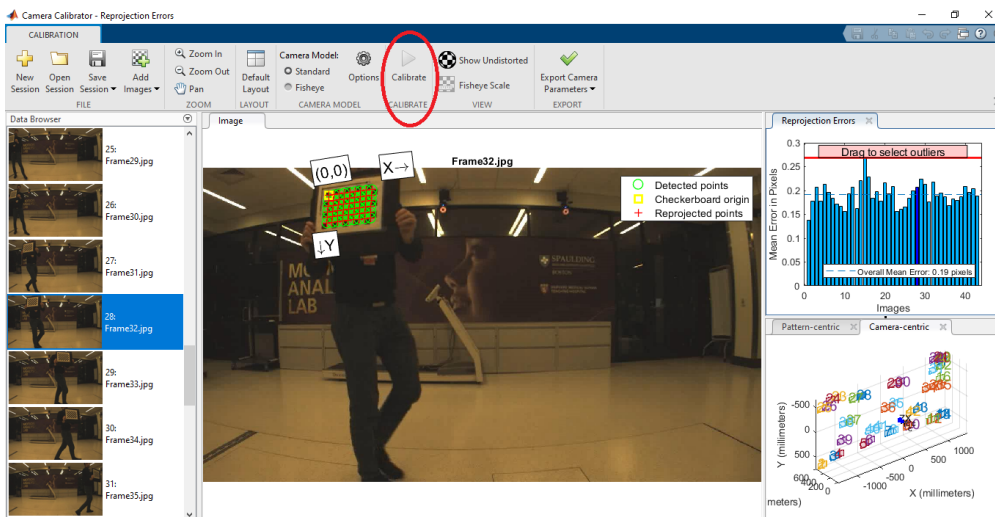


Figure B.5: Calibration of the instrument

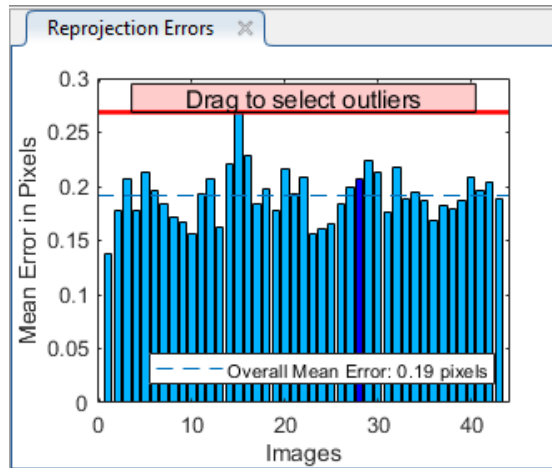


Figure B.6: Results in term of reprojection errors

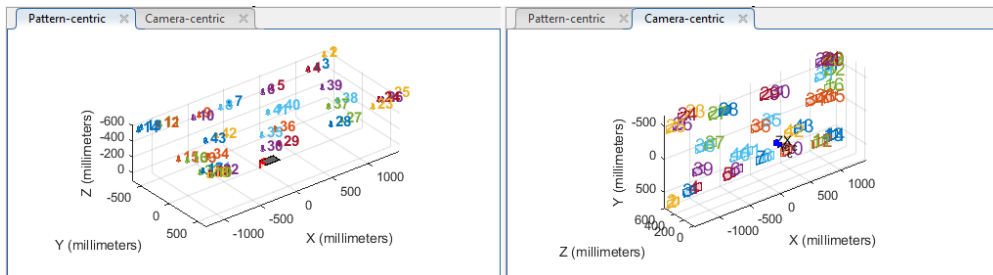


Figure B.7: Results in term of camera and pattern centric

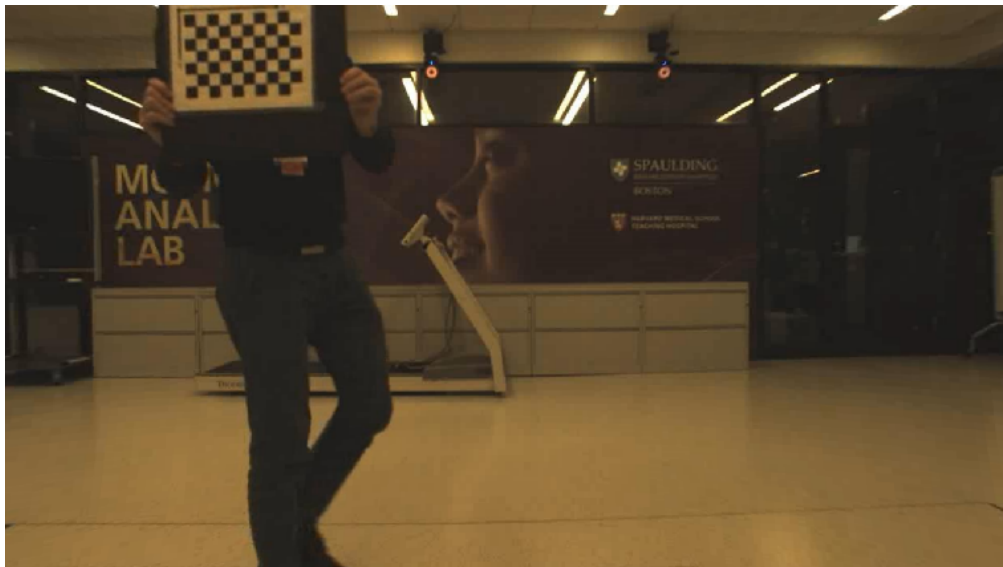


Figure B.8: Image without distortions

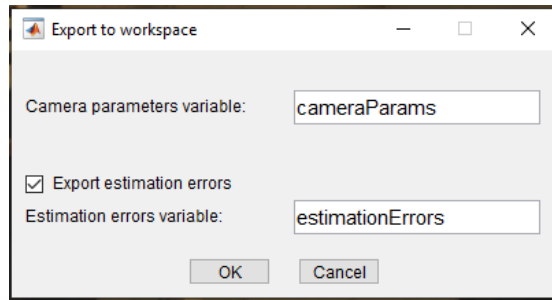


Figure B.9: Export of calculated final parameters

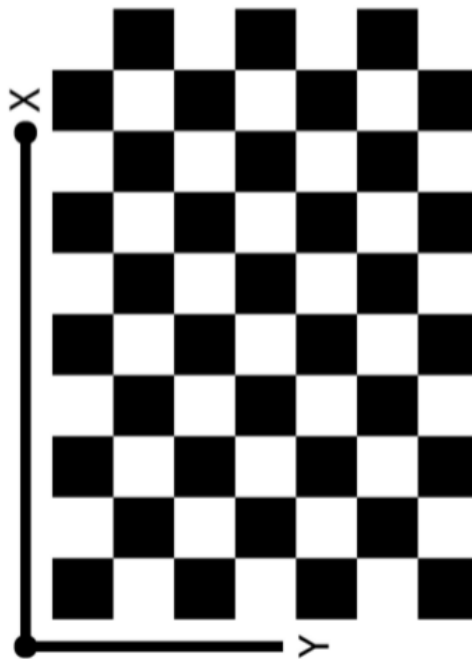


Figure B.10: An example of chessboard that can be used for the calibration of the Bonita cameras

Bibliography

- [1] Ashutosh Kharb, Vipin Saini, YK Jain, and Surender Dhiman. «A review of gait cycle and its parameters». In: *IJCEM International Journal of Computational Engineering & Management* 13 (2011), pp. 78–83 (cit. on p. 3).
- [2] A. Bonnefoy-Mazure and Stéphane Armand. «Normal gait». In: Jan. 2015, pp. 199–214 (cit. on p. 4).
- [3] Perry Jacquelin; Burnfield Judith. *Gait Analysis: Normal and Pathological Function*. SLACK Incorporated, 2010 (cit. on p. 3).
- [4] Los Amigos Research, Inc Education Institute, Rancho Los Amigos National Rehabilitation Center, Rancho Los Amigos National Rehabilitation Center. Pathokinesiology Service, and Rancho Los Amigos National Rehabilitation Center. Physical Therapy Department. *Observational Gait Analysis*. Los Amigos Research and Education Institute, Rancho Los Amigos National Rehabilitation Center, 2001. ISBN: 9780967633510. URL: <https://books.google.it/books?id=sZdMPgAACAAJ> (cit. on p. 3).
- [5] G. Malanga and A. Delisa. «Clinical Observation». In: 2005 (cit. on p. 5).
- [6] Jacqueline J. Wertsch Gerald F. Harris. «Procedures for Gait Analysis». In: *Archives of Physical Medicine and Rehabilitation* 75 (1994), pp. 216–225 (cit. on p. 7).
- [7] Alvaro Muro-de-la-Herran, Begonya Garcia-Zapirain, and Amaia Mendez-Zorrilla. «Gait Analysis Methods: An Overview of Wearable and Non-Wearable Systems, Highlighting Clinical Applications». In: *Sensors* 14.2 (Feb. 2014), pp. 3362–3394. ISSN: 1424-8220. DOI: 10.3390/s140203362. URL: <http://dx.doi.org/10.3390/s140203362> (cit. on p. 7).
- [8] Amod Kumar Neelesh Kumar Nissan Kunju and B.S. Sohi. «Active marker based kinematic and spatio-temporal gait measurement system using LAB VIEW vision». In: *Journal of Scientific & Industrial Research* 69 (2010), pp. 600–605 (cit. on pp. 9, 11).

- [9] «Calibration Motion Capture Accessories». In: Available on line. URL: <https://www.vicon.com/products/vicon-devices/calibration> (cit. on pp. 13, 14).
- [10] «Vicon Nexus User Guide». In: Available on line. URL: <https://docs.vicon.com/> (cit. on p. 14).
- [11] «Creating labeling skeleton templates (VSTs)». In: Available on line. URL: <https://docs.vicon.com/> (cit. on pp. 14, 16).
- [12] «Plug-in Gait Reference Guide». In: Available on line. URL: <https://docs.vicon.com/> (cit. on p. 17).
- [13] Zhe Cao, Gines Hidalgo, Tomas Simon, Shih-En Wei, and Yaser Sheikh. «OpenPose: Realtime Multi-Person 2D Pose Estimation using Part Affinity Fields». In: *CoRR* abs/1812.08008 (2018). arXiv: 1812.08008. URL: <http://arxiv.org/abs/1812.08008> (cit. on pp. 18–22, 24, 69, 70).
- [14] MATLAB. *version 7.10.0 (R2019b)*. Natick, Massachusetts: The MathWorks Inc., 2010 (cit. on pp. 27, 71).
- [15] J.Y. Bouguet. «Matlab Camera Calibration Toolbox». In: 2000 (cit. on pp. 27–30, 71).
- [16] Nobuyasu Nakano, Tetsuro Sakura, Kazuhiro Ueda, Leon Omura, Arata Kimura, Yoichi Iino, Senshi Fukashiro, and Shinsuke Yoshioka. «Evaluation of 3D markerless motion capture accuracy using OpenPose with multiple video cameras». In: *bioRxiv* (2019). DOI: 10.1101/842492. eprint: <https://www.biorxiv.org/content/early/2019/11/15/842492.full.pdf>. URL: <https://www.biorxiv.org/content/early/2019/11/15/842492> (cit. on p. 47).
- [17] Heather Read, M Hazlewood, Susan Hillman, Robin Prescott, and James Robb. «Edinburgh Visual Gait Score for Use in Cerebral Palsy». In: *Journal of pediatric orthopedics* 23 (May 2003), pp. 296–301. DOI: 10.1097/01241398-200305000-00005 (cit. on pp. 64, 65).
- [18] *CMU-Perceptual-Computing-Lab*. URL: <https://github.com/CMU-Perceptual-Computing-Lab/openpose> (visited on 2019) (cit. on pp. 64, 66, 69).